

**Narrow-Angle Astrometry with the Space Interferometry Mission:
The Search for Extra-Solar Planets.**

II. Detection and Characterization of Planetary Systems

A. Sozzetti^{1,2,3}

alex@phyast.pitt.edu

S. Casertano⁴ and R. A. Brown⁴

stefano@stsci.edu; rbrown@stsci.edu

and

M. G. Lattanzi³

lattanzi@to.astro.it

ABSTRACT

We utilize *a*) detailed end-to-end numerical simulations of sample narrow-angle astrometric observing campaigns with the Space Interferometry Mission (SIM) and the subsequent data analysis process, and *b*) the set of extra-solar planetary systems discovered so far by radial velocity surveys as templates to provide meaningful estimates of the limiting capabilities of SIM for the detection and measurement of multiple-planet systems around solar-type stars in the solar neighborhood.

We employ standard χ^2 statistics, periodogram and Fourier analysis to evaluate SIM's ability to detect multiple planetary signatures: the probability of detecting additional companions is essentially unchanged with respect to the single-planet configurations, but after fitting and subtraction of orbits with astrometric signal-to-noise ratio $\alpha/\sigma_d \rightarrow 1$ the false detection rates can be enhanced by up to a factor 2; the periodogram approach results in robust multiple-planet detection for systems with periods shorter than the SIM mission length, even at low values of α/σ_d , while the least squares technique combined with Fourier series expansions is arguably preferable in the long-period regime. We explore the three-dimensional parameter space defined by astrometric signature, orbital period, and eccentricity to derive general conclusions on the

¹University of Pittsburgh, Dept. of Physics & Astronomy, Pittsburgh, PA 15260, USA

²Smithsonian Astrophysical Observatory, Harvard-Smithsonian Center for Astrophysics, 60 Garden Street, Cambridge, MA 02138

³Osservatorio Astronomico di Torino, 10025 Pino Torinese, Italy

⁴Space Telescope Science Institute, Baltimore, MD 21218, USA

capability of SIM to accurately measure the full set of orbital parameters and masses for a variety of configurations of planetary systems: the accuracy on multiple-planet orbit reconstruction and mass determination suffers a typical degradation of 30-40% with respect to single-planet solutions; mass and orbital inclination can be measured to better than 10% for periods as short as 0.1 yr, and for α/σ_d as low as ~ 5 , while $\alpha/\sigma_d \simeq 100$ is required in order to measure with similar accuracy systems harboring objects with periods as long as three times the mission duration. We gauge the potential of SIM for meaningful coplanarity measurements via determination of the true geometry of multiple-planet orbits: for systems with all components producing $\alpha/\sigma_d \simeq 10$ or greater, quasi-coplanarity can be reliably established with uncertainties of a few degrees, for periods in the range $0.1 \leq T \leq 15$ yr; in systems where at least one component has $\alpha/\sigma_d \rightarrow 1$, coplanarity measurements are compromised, with typical uncertainties on the mutual inclinations of order of $30^\circ - 40^\circ$. We quantify the improvement derived in full-orbit reconstruction and planet mass determination by constraining the multiple-planet orbital fits to SIM observations with the nominal orbital elements obtained from the radial velocity measurements: the uncertainties on orbital elements and masses can be reduced by up to an order of magnitude, especially for long-period orbits in face-on configurations, and for low amplitude orbits seen edge-on.

Our findings are illustrative of the importance of the contribution SIM will make, complementing other on-going and planned spectroscopic, astrometric, and photometric surveys, in order to fulfill the expectations for ground-breaking science in the fields of formation and evolution of planetary systems during the next decade.

Subject headings: astrometry – planetary systems – instrumentation: interferometers – methods: data analysis – methods: numerical

1. Introduction

After more than thirteen years of precise radial velocity measurements, today there is clear evidence that several nearby solar-type stars harbor candidate planetary systems, composed of two or more planets (Butler et al. 1999; Marcy et al. 2001b; Mayor et al. 2001; Jones et al. 2002; Fischer et al. 2002; Marcy et al. 2002b; Fischer et al. 2003; Butler et al. 2003), or a planet and a probable brown dwarf (Marcy et al. 2001a; Udry et al. 2002)

The answers provided by these discoveries have presented even more challenging puzzles to theoretical models aimed at describing the formation and evolution of planetary systems. The variety of orbital arrangements in multiple-planet systems found by spectroscopy calls into question both the origin and early dynamical evolution of such systems, in terms of formation mechanisms and orbital migration scenarios, as well as their long-term dynamical evolution and stability. Early attempts have been made to connect and relate the early stages of their formation

to their presently observed orbital properties. For example, the two planets orbiting the M4V star Gliese 876 appear to be locked in a 2:1 resonance, and the existence of such commensurabilities may be considered important evidence of possible inward migration for pairs of planets due to mutual interactions as well as tidal interaction with the protoplanetary disk during and shortly post-formation (Snellgrove et al. 2001; Nelson & Papaloizou 2002). Similarly, the three-planet system around the F8V star ν Andromedæ (ν And) appears to be stable over evolution timescales of order of the star’s lifetime, again suggesting the possibility that the system’s orbits were shaped by the interaction of protoplanets with the protoplanetary disk, in the first few million years of ν And’s existence (Artymowicz 2001). Furthermore, in many of the observed multiple-planet systems the eccentricities are much larger than those of the planets of our own solar system. Again, this may be explained with significant eccentricity evolution due to mutual interaction between planets as well as with the protoplanetary disk during the epoch of disk depletion (Chiang & Murray 2002; Nagasawa et al. 2003). However, direct extrapolations from the early stages of their formation to the presently observed configurations of extra-solar planetary systems are still somewhat speculative. Today, in fact, there is still a lack of observational support to the theoretical models describing the early epochs of the formation of planetary systems, either because of the objective difficulty to identify good targets among very young stellar objects (often completely obscured by circumstellar material) or due to insufficient sensitivity of the present generation of ground-based and space-borne instrumentation. Thus, theorists have focused primarily on the issues of long-term stability and orbital evolution of extra-solar planetary systems, independent on the details of their formation.

Since Newton’s discovery of the law of universal gravitation, the problem of predicting the orbits of the planets in our own solar system has been tackled by many giants of mathematics (Euler, Laplace, Jacobi, Lagrange, Gauss, Poincaré). By the end of the nineteenth century, it had been demonstrated that it is not possible to find an exact analytic solution describing the motion of N bodies, for $N \geq 3$, and the theory of perturbations in celestial mechanics was developed and extensively applied to many interesting cases, always within the boundaries of our solar system. During the two last decades, with the advent and exponential progress of computer technology, large-scale computations that follow the full evolution of the nine planets for a significant fraction of the lifetime of the Sun became possible. This has allowed the establishment of, for example, the long-term chaotic behavior of the orbits of planets in the solar system (Sussman & Wisdom 1992). In fact, the typical (Lyapunov) timescale for exponential divergence of two orbits in the solar system starting with slightly different initial conditions is only several million years, and soon the issue of stability only becomes a statistical question. The planetary orbits in the solar system are on the other hand stable, in the sense that the probability of ejections or close encounters during a time frame comparable to the main-sequence lifetime of the Sun (~ 12 Gyr) is extremely low.

However, until the first multiple-planet system was announced (Butler et al. 1999), the problem of planetary orbits dynamics had in recent years been almost relegated to the level of an academic pursuit. Now that a variety of additional systems, with a wide range of different orbital

arrangements, has been found, the field of planetary system dynamics has received revived interest. The long-term dynamical evolution of the 11 extra-solar planetary systems known to date has been extensively investigated by theorists, utilizing both direct numerical integrations and approximate analytical approaches for the description of the N-body mutual interactions. As opposed to our own solar system, or the three-planet system discovered by Wolszczan & Frail (1992) around the pulsar PSR 1257+12, both appearing dynamically stable over long timescales (Laskar 1994; Gladman 1993), the dynamical evolution and long-term stability issues for the majority of the multiple-planet systems discovered by radial velocity are highly uncertain. As a general result, studies specifically targeted to gauge the general dynamical behavior of extra-solar planetary systems such as ν And (Laughlin & Adams 1999; Rivera & Lissauer 2000; Stepinski et al. 2000; Jiang & Ip 2001; Barnes & Quinn 2001; Chiang et al. 2001; Rivera & Lissauer 2001a, Chiang & Murray 2002), 55 Cancri (55 Cnc hereafter. Novak et al. 2002; Ji et al. 2003), 47 Ursæ Majoris (47 UMa hereafter. Godzdziewski 2002; Laughlin et al. 2002), Gliese 876 (Kinoshita & Nakai 2001; Laughlin & Chambers 2001; Rivera & Lissauer 2001b; Ji et al. 2002a; Godzdziewski et al. 2002; Lee & Peale 2002a, 2002b), HD 82943, HD 37124, HD 12661, HD 38529, and HD 160691 (Godzdziewski & Maciejewski 2001; Kiseleva-Eggleton et al. 2002; Godzdziewski & Maciejewski 2003; Godzdziewski 2003a, 2003b), come to the same conclusion: the stability of the systems can be greatly affected by small variations of the instantaneous orbital elements of the planetary orbits obtained from the radial velocity data and utilized as initial conditions for the numerical integrations. In particular, for the systems not to be destabilized and disrupted on very short timescales (as short as 10^3 - 10^5 years), constraints must be placed on the maximum allowed values for the masses and on the range of allowed relative inclinations of the orbits. Often analytical calculations are performed with the coplanarity of the orbits as a working assumption. Early attempts have also been made to verify the possibility of regions of dynamical stability inside the parent stars' Habitable Zones (Kasting et al. 1993), where Earth-size planets may be found (Jones et al. 2001; Noble et al. 2002; Jones & Sleep 2002a, 2002b; Rivera & Haghighipour 2002; Cuntz et al. 2003; Menou & Tabachnik 2003). However, the existence of such regions does not directly imply that rocky planets may have actually formed, in these systems, at such privileged distances, in the first place (Thébaud et al. 2002).

The results obtained by many of the present studies on the dynamical stability of extra-solar planetary systems contain significant ambiguities. The impossibility to draw at present more than general statistical conclusions on such issues arises partly from the intrinsically chaotic nature of N-body systems, and partly from a lack of knowledge of a few key parameters that cannot be derived by the present observational datasets, but must be *a priori* fixed throughout the analyses. As a matter of fact, in general four quantities drive the effects of the mutual perturbations in multiple-planet systems investigated by theorists: the planetary eccentricities, the orbital periods (and possible commensurabilities among them), the planet masses (usually through their ratio), and the relative inclinations of the orbital planes. The last two of these parameters cannot be determined from the intrinsically one-dimensional information extracted from stellar spectra. In fact, radial velocity measurements do not determine either the inclination i of the orbital plane with

respect to the plane of the sky (and this in turn allows only for lower limits to be placed on the actual mass of each companion to the observed star) or the position angle Ω of the line of nodes in the plane of the sky (and thus relative inclination angles remain unknown): without knowledge of the full three-dimensional geometry of the systems and true mass values, general conclusions on the architecture, orbital evolution and long-term stability of the newly discovered planetary systems remain questionable.

Attempts have been made to break the $\sin i$ degeneracy and determine the true masses of planets in multiple systems utilizing self-consistent dynamical fits (Laughlin & Chambers 2001; Rivera & Lissauer 2001b). Such procedures significantly improve orbital fits performed assuming independent Keplerian motions in cases such as that of Gliese 876, where mutual perturbations are relevant and the orbital elements of the planets undergo significant changes on timescales comparable to the timespan of the observations. However, these dynamical fits to the radial velocity data are not conclusive, as assumptions must still be made on the actual relative inclinations of the planets, and broad ranges of $\sin i$ provide similarly good fits. Thus, tightly constraining planetary masses will be difficult for several years to come, if one has to rely only upon radial velocity measurements. Furthermore, different orbital configurations giving similarly good values of the reduced chi-square $\chi_\nu^2 = \chi^2/\nu$ (where ν is the number of degrees of freedom) behave very differently when integrated over long timescales, and the ambiguity on the actual long-term stability of the systems cannot be removed.

In the latest years other techniques have reached the sensitivity necessary to complement spectroscopy in extra-solar planet searches. In particular, transit photometry has been successful in identifying the first gas giant planet eclipsing its parent star (Charbonneau et al. 2000; Henry et al. 2000), confirming the spectroscopic detection (Mazeh et al. 2000; Queloz et al. 2000), and very recently in directly discovering the second transiting planet (Konacki et al. 2003). The observations of planetary transits on the disk of HD 209458 allow for a direct estimate of the planet's size and actual mass (as the inclination of the orbital plane is known, and the $\sin i$ degeneracy breaks down), thus, also thanks to the recent detection of sodium in its atmosphere (Charbonneau et al. 2002), its density can be inferred and important insights on its composition can be obtained. However, transit photometry detects only the small proportion of planets whose orbits happen to line up almost exactly with the line of sight to the star. We anticipate that future high-precision ground-based (Mariotti et al. 1998; Booth et al. 1999; Colavita et al. 1999) as well as space-borne (Danner & Unwin 1999; Perryman et al. 2001) astrometric observatories will be among the most effective techniques to remove the present ambiguities in the dynamical analysis of extra-solar planetary systems as well as provide valuable data to probe models addressing the issues of the formation of planetary systems and the actual nature of sub-stellar companions. The intrinsically two-dimensional astrometric data provide the means to directly measure the two missing parameters, i.e. the inclination angle and the line of nodes of each planetary orbit. Knowledge of the full viewing geometry of a system of planets allows then to derive meaningful estimates for the true masses of each orbiting object and the relative inclinations of the orbital planes.

In our previous work (Sozzetti et al. 2002, S02 hereafter), we addressed the issues of the detectability and measurability of single planets around single stars with the Space Interferometry Mission (SIM), with the instrument operated in narrow-angle astrometric mode. We expressed our results as a function of both SIM mission parameters and properties of the planet (mass, orbital characteristics). In the continuation of our studies we have utilized extensive simulations of SIM observations of the present sample of extra-solar multiple-planet systems in order to draw general conclusions on the ability of SIM to discover and measure systems of planets, as well as quantify the instrument’s capability to determine the coplanarity of multiple-planet orbits. Similarly, Sozzetti et al. (2001) have recently assessed the capabilities of ESA’s Cornerstone Mission GAIA for the detection and measurement of planetary systems utilizing the ν And system as a template. Our study is different in that, addressing the entire set of presently known multiple-planet systems, it extends the analysis beyond the favorable cases (well-spaced, well-sampled orbits, high “astrometric” signal-to-noise ratios) studied by Sozzetti et al. (2001), and is specifically tailored to SIM.

This second paper is organized as follows. In the second Section we briefly describe the setup for the simulation of SIM sample narrow-angle campaigns, the statistical tools implemented for planet detection, and the algorithms for multiple orbital fits. In the third Section we present results on multiple-planet systems detection, multiple-planet orbit reconstruction, and coplanarity analyses, and compare our results to those of previous studies. Finally, in the fourth Section we summarize our results and discuss our findings in the context of the present status of planet searches.

2. Simulation Setup, Detection and Orbital Fitting Methods

The code for the reproduction of sample observing campaigns with SIM operated in narrow-angle astrometric mode and the subsequent analysis of the simulated dataset has been thoroughly described in S02, where we defined detectability horizons and limits on distance for accurate orbital parameters and mass determination in the case of single planets orbiting single, nearby solar-type stars. In this Section we summarize its main features and working assumptions, and describe the modifications made in order to address the issues of multiple-planet system observations, detection, and measurement.

2.1. SIM Narrow-Angle Astrometric Observing Scenario

The SIM instrument (for a thorough presentation of the mission concept see for example Danner & Unwin 1999) executes pointed observations at arbitrary times and orientations of the interferometric baseline. When operating in the regime of narrow-angle astrometry, its fundamental one-dimensional measurement is the *relative* optical path-length delay:

$$\Delta d_{\star,n} = \mathbf{B} \cdot (\mathbf{S}_{\star} - \mathbf{S}_n) + \sigma_d \quad (1)$$

which corresponds to the instantaneous angular distance between the target and its n -th reference star, projected onto the baseline of the science interferometer, while the two guide interferometers accurately monitor changes in the satellite’s attitude by acquiring fringes of two bright guide stars. In the above formula $\mathbf{B} = B\mathbf{u}_b$ is the interferometer baseline vector of length B , \mathbf{S}_\star and \mathbf{S}_n are the unit vectors to the target star and its n -th reference object, while σ_d is the single-measurement accuracy on each relative delay measurement.

Throughout all our simulations we have adopted the template observing scenario outlined in S02: within a domain of 1° in diameter around each target we place $N_r = 3$ reference stars, and execute $N_o = 24$ full two-dimensional observations (corresponding to a total of $N_m = 144$ relative delay measurements) randomly, uniformly distributed over the nominal $L = 5$ years mission lifetime, each composed of two one-dimensional standard visits made with orthogonal orientations of the interferometer baseline vector. Since in our study we have utilized the present set of extra-solar planetary systems, orbiting very bright ($V \leq 10$ mag), nearby, solar-type stars (spectral types F-G-K, except for Gliese 876), we have utilized a structure of the standard visit which applies to bright target and reference stars ($V \leq 11$ mag), and consequently set a single-measurement error $\sigma_d = 2 \mu\text{as}$ throughout all our analysis (see S02 for details on the adopted error model). This value for σ_d is in line with the presently envisaged SIM performance in its new shared-baseline configuration.⁵

The basic assumptions made in our previous work with regard to the SIM instrument and the systems to be investigated are unchanged in this study: 1) we assume perfect knowledge of the error model and attitude of the spacecraft; 2) the objects composing the local frame of reference, with respect to which observations of a given scientific target are made, are assumed astrometrically clean, i.e. sources of astrometric noise intrinsic to the source, such as flares, rotating spots, or marginally unstable circumstellar disks, have not been taken into consideration, nor have we discussed the possibility of binaries among either targets or reference stars; 3) effects on the targets’ displacement due to perspective acceleration, changing parallax, or higher-order contributions from relativistic aberration and light deflection from the major solar system bodies have not been included.

We have modified the description of the target motion on the celestial sphere to allow for the presence of multiple planets. The stellar motion is described in terms of the 5 basic astrometric parameters and of the gravitational perturbations produced by the orbiting planets. The difference between the position vector to the target \mathbf{S}_\star evaluated at time t and the same quantity \mathbf{S}'_\star measured at time t' can then be expressed as a sum of small perturbative terms:

$$\mathbf{S}'_\star - \mathbf{S}_\star = d\mathbf{S}_\star = d\mathbf{S}_\mu + d\mathbf{S}_\pi + \sum_{i=1}^{n_p} d\mathbf{S}_K^i, \quad (2)$$

where n_p is the number of planets orbiting the target. The gravitational effects produced by

⁵The results presented and discussed in the following Sections can easily be rescaled to different timing and numbers of full-observations and reference stars, with the simple scaling laws already derived in S02

the planets are assumed to be linear (i.e., as the sum of independent Keplerian motions). Such simplification (no mutual gravitational interactions between planets) has in general little impact on the significance of our analysis. In fact, assuming the orbits are coplanar, over the time-scale of SIM observations (5 years), variations of the orbital parameters due to secular as well as resonant perturbative terms can be confidently considered negligible. This assumption may not be correct only in the case of Gliese 876, where the two gas giant planets orbiting the star are locked in a 2:1 resonance, and strong mutual perturbations are already evident in the data over the timescale of the radial velocity observations (~ 13 years). We plan to study in detail in a future work the effects induced by mutual gravitational perturbations between planets on the quality of multiple-planet orbital fits that do and do not contain analytic descriptions of the resonant and/or secular perturbative nature of the systems.

2.2. Statistical Tools for Planet Detection

We adopt two different procedures for investigating the efficiency of SIM in detecting multiple-planet systems.

First of all, following the approach in S02, we employ a standard χ^2 test with confidence level set to 95% applied to the observation residuals. The test is performed initially against the null hypothesis that there is no planet, then after removal of the first planetary signature it is applied in succession until no further significant deviations (at the 95% confidence level) from the fitted model containing n_p planets appear in the residuals.

Secondly, we have upgraded our code to include a basic periodogram analysis in order to search for hidden periodicities in the astrometric measurements. To this aim, we have utilized the standard algorithm for the evaluation of the Lomb-Scargle normalized periodogram for the spectral analysis of unevenly sampled data (Press et al. 1992), specifically its ‘fast’ version by Press & Rybicki (1989). The traditional Lomb-Scargle formula is equivalent to performing an unweighted linear least-squares fit of a sinusoid to the data, after subtraction of the mean. For a time series of relative delays $\Delta d(t_i)$, where i takes on integer values up to the total number of measurements N_m , the normalized periodogram as a function of the test angular frequency ϑ is defined as:

$$z(\vartheta) = \frac{1}{2\sigma_d^2} \left\{ \frac{\left[\sum_{i=1}^{N_m} (\Delta d(t_i) - \overline{\Delta d}) \cos \vartheta(t_i - t_c) \right]^2}{\sum_{i=1}^{N_m} \cos^2 \vartheta(t_i - t_c)} + \frac{\left[\sum_{i=1}^{N_m} (\Delta d(t_i) - \overline{\Delta d}) \sin \vartheta(t_i - t_c) \right]^2}{\sum_{i=1}^{N_m} \sin^2 \vartheta(t_i - t_c)} \right\} \quad (3)$$

Here, $\overline{\Delta d}$ is the mean of the data, while t_c is given by

$$t_c = \frac{1}{2\vartheta} \arctan \left(\frac{\sum_{i=1}^{N_m} \sin 2\vartheta t_i}{\sum_{i=1}^{N_m} \cos 2\vartheta t_i} \right) \quad (4)$$

The normalization factor is by default taken as the variance of the sample. Because of the exploratory nature of this investigation, we assign equal weight to all observations and set $\sigma_d = 2$

μas , the value of the single-measurement error on relative delays as defined in the previous Section. At the moment we do not discuss the merit of other possible choices for the normalization of the periodogram (Gilliland & Baliunas 1987; Schwarzenberg-Czerny 1996).

Observation residuals are inspected successively after the single-star fit, and after removal of each planetary signature, to establish the existence or absence of further periodicities. Also in this case, the significance of the detection or non detection of a periodic signal in the residuals, i.e. the significance of a particular peak in the power spectrum $z(\vartheta)$, must be assessed. For the above choice of the normalization factor, the probability that a periodogram power z is above some value z_0 is then $P(z > z_0) = e^{-z_0}$ (Scargle 1982; Horne & Baliunas 1986), and, if M independent frequencies are scanned, the probability that none gives values larger than z_0 is $(1 - e^{-z_0})^M$. Then, the *false-alarm probability* of the null hypothesis that the data are pure noise is computed for each value of z as:

$$P(> z_0) = 1 - (1 - e^{-z_0})^M \quad (5)$$

This expression provides an estimate of the significance of each given peak in the spectrum that can be identified. For sufficiently high values of z_0 the false-alarm probability is very small, and this corresponds to the detection of a highly significant periodic signal.

The choice of M is critical in assessing the true significance of a given peak in the spectrum. In general, the larger the number of frequencies, the less significant is any ‘bump’ in the periodogram power. The actual value of M depends in general on the actual frequency range scanned, and on the number and clumpiness of the data points available for the investigation. For this reasons, it is difficult to derive a closed analytical form for the number of independent frequencies. For period searches between the average Nyquist period ($T_{\text{Nyq}} \simeq 2L/N_m$) and the duration of the data set a reasonable choice is $M \simeq N_m$ (Horne & Baliunas 1986). However, when sampling very short periods, in general frequencies much higher than the average Nyquist frequency are reached, then the number of independent frequencies will be higher. For any particular case, an actual value of M can be estimated by simple Monte Carlo analysis: holding fixed the number and epochs of the observations, generate synthetic datasets containing only Gaussian (normal) noise representative of the actual errors, then find the largest value of $P(> z_0)$ and fit the resulting distribution for M in Eq. 5. By doing so, Marcy & Benitz (1989) and Cumming et al. (1999) derive $M = 1.15N_m$ and $M = 1.175N_m$, respectively, and this may be compared with the analytic relation $M = -6.4 + 1.19N_m + 0.00098N_m^2$ by Horne & Baliunas (1986). Given the illustrative purpose of our analysis, we rely on results from the literature and choose a typical value $M = 1.20N_m$ throughout our simulations.

2.3. Procedure for Multiple-Planet Orbital Fits

The iterative method for the solution of the non-linear systems of equations of condition is based on a slightly modified version of the Levenberg-Marquardt algorithm, as described in S02,

which ensures stability of the solution. It has been upgraded to allow for the presence of multiple, independent planetary perturbations.

The photocenter motion of the target is described by an analytical model in which the re-computed relative delay between the target and its j -th reference star ($j = 1, \dots, N_r$) is in the form:

$$\begin{aligned} \Delta d_{\star,j} = & \mathbf{B} \cdot (\mathbf{S}_\star(\lambda_\star, \beta_\star, \mu_{\lambda,\star}, \mu_{\beta,\star}, \pi_\star, \sum_{l=1}^{n_p} (X_{1,l}, X_{2,l}, X_{3,l}, X_{4,l}, e_l, T_l, \tau_l)) \\ & - \mathbf{S}_j(\lambda_j, \beta_j, \mu_{\lambda,j}, \mu_{\beta,j}, \pi_j)) \end{aligned} \quad (6)$$

The five astrometric parameters (two positions, two proper motion components, and parallax) of the target ($\lambda_\star, \beta_\star, \mu_{\lambda,\star}, \mu_{\beta,\star}, \pi_\star$) and each of the N_r local reference objects ($\lambda_j, \beta_j, \mu_{\lambda,j}, \mu_{\beta,j}, \pi_j$) are defined in ecliptic coordinates (see S02 for details), while for the seven orbital elements needed to describe the orbit of each of the n_p planets around the target we have utilized the Thiele-Innes representation, in which the semi-major axis a_l , the inclination i_l , the longitude of pericenter ω_l and the position angle of the line of nodes Ω_l of the l -th planet are combined to form the quantities:

$$\begin{aligned} X_{1,l} &= a_l(\cos \omega_l \cos \Omega_l - \sin \omega_l \sin \Omega_l \cos i_l) \\ X_{2,l} &= a_l(-\sin \omega_l \cos \Omega_l - \cos \omega_l \sin \Omega_l \cos i_l) \\ X_{3,l} &= a_l(\cos \omega_l \sin \Omega_l + \sin \omega_l \cos \Omega_l \cos i_l) \\ X_{4,l} &= a_l(-\sin \omega_l \sin \Omega_l + \cos \omega_l \cos \Omega_l \cos i_l) \end{aligned}$$

In this model, the observation equations are strictly nonlinear only in the orbital period T_l , the eccentricity e_l , and the epoch of pericenter passage τ_l . At the end of each simulation, the classic orbital parameters are recomputed from the Thiele-Innes elements (see for example Heintz 1978). The mass $M_{p,l}$ of the l -th planet is then determined by combining the values of T_l (in years), π_\star and the semi-major axis of the stellar orbit around the barycenter of the system $a_{\star,1}$ (both in arcseconds), all estimated from the fit to the observed delays, and the stellar mass M_\star , assumed perfectly known, in the following approximation of the mass-function formula for $M_{p,l} \ll M_\star$:

$$M_{p,l} \simeq \left(\frac{a_{\star,1}^3 M_\star^2}{\pi_\star^3 T_l^2} \right)^{1/3} \quad \text{for } l = 1, \dots, n_p \quad (7)$$

The multiple-orbit fitting procedure also determines the formal errors on each estimated parameter x_m as:

$$\sigma(x_m) = \sqrt{C_{mm}}, \quad (8)$$

where the C_{mm} 's are the diagonal elements of the covariance matrix of the fit (Press et al. 1992). In the case of the orbital parameters recomputed from the Thiele-Innes elements and the mass of

each planet, formal errors are propagated utilizing the classic error propagation formula, including correlations between the measured parameters:

$$\sigma(z_k) = \sqrt{\sum_{i=1}^{m_f} \sum_{j=1}^{m_f} \frac{\partial z_k}{\partial x_i} \frac{\partial z_k}{\partial x_j} \sigma(x_i) \sigma(x_j)}, \quad (9)$$

where the sums are extended to the m_f fitted parameters from which the k -th recomputed quantity z_k depends.

As already highlighted in S02, convergence of the non-linear fitting procedure and quality of the orbital solutions can both be significantly affected by the choice of the starting guesses. In the studies presented here this issue has been left aside because, focusing on the set of presently known planetary systems, we have utilized as starting guesses the values of the orbital parameters for the planets in each system published in the literature. Nevertheless, whenever data will be inspected to search for planetary signatures in the absence of *a priori* information on the actual presence of planets around a given target, important questions will have to be addressed and answered, related to how and to what extent effective starting values, i.e., leading to successful orbital solutions, will be identified from the data as a function of actual instrument performances, uncertainties in the error model, and intrinsic properties of the planetary systems. To this end, realistic global search strategies will have to be tested and double-blind test campaigns conducted. Work on these issues is in progress and will be reported in the future.

3. Results

In addressing the problem of the detection and measurement of multiple planets with SIM, we have utilized the entire set of existing planetary systems known to date as representative test cases. The results are discussed below, as follows. First, we study SIM’s efficiency in multiple-planet detection by means of a method that combines standard χ^2 statistics, periodogram analysis and Fourier series expansions. Next, we estimate SIM’s ability to make accurate measurements of multiple-planet orbits and masses. Then, we gauge the boundaries of SIM’s capability to determine the coplanarity of the orbits of planets in systems. Finally, we quantify how beneficial it would be to be able to combine astrometric and spectroscopic orbital elements in order to improve the accuracy in full-orbit reconstruction, planet mass determination, and coplanarity measurements. All results reported here have been obtained assuming end-of-mission analysis of the simulated datasets. We do not discuss in this paper modifications to the strategy for the analysis of SIM observations at earlier stages of the mission, when the instrument operations are still ongoing.

3.1. Detectability of Multiple-Planet Systems

In this Section we focus on establishing the boundaries of reliable multiple-planet system detection with SIM for a wide range of orbital arrangements, including low values of the astrometric signal-to-noise ratio α/σ_d and orbital periods exceeding the mission lifetime. To this end, we have investigated the performances of various detection methods (χ^2 test, Fourier series, periodogram analysis) in the different regimes. Our study is primarily illustrative, and clearly does not cover all possible arrangements of planetary systems, such as configurations with extreme orbital shapes and orientations, and small amplitudes of the astrometric signal (either because of small planet masses, or due to large distances).

3.1.1. Probabilities of Detection

As discussed in S02, the easiest way to quantify SIM’s sensitivity to planetary perturbations is to parameterize it through the orbital period T and the *astrometric signal-to-noise ratio* α/σ_d , where σ_d is the single-measurement error on each relative delay measurement, while the *astrometric signature* α is the apparent amplitude of the gravitational perturbation induced on the observed star by a single companion, defined as:

$$\alpha = \frac{M_p a_p}{M_\star D}, \quad (10)$$

where M_p , M_\star are the masses of the planet and star respectively (in solar masses), a_p the semi-major axis of the planetary orbit (in AU), D the distance of the system from the observer (in pc). In the case of multiple, independent Keplerian perturbations, the orbital motion of the star about the barycenter will contain components reflecting the orbital periods of each of the companions, with the peak amplitude corresponding to the object with the larger value of the product $M_p \times a_p$ (for a given distance of the system and mass of the central star). It must be noted that Eq. 10 constitutes only an upper limit to the actual magnitude of the measured perturbation, without any projection or eccentricity effect. If the plane of a circular orbit lies in the plane of the sky, the two projections of the perturbation will be equal, with amplitudes given by Eq. 10. If the orbital plane is inclined with respect to the line of sight, there will always be some projection of the orbit on the plane of the sky which has the amplitude given by Eq. 10, but the amplitude at other positions angles will be less. If the orbit is eccentric, there could be cases where the orientation of the orbital plane with respect to the observer’s line of sight gives rise to significantly smaller apparent amplitudes than indicated in Eq. 10: in the worst-case scenario, when the line of apsides is aligned with the line of sight the maximum measured amplitude corresponds to the orbital semi-minor axis, which is still equal to $> 0.95 a_p$ for moderately eccentric orbits ($e < 0.3$), but can drop below $0.5 a_p$ for high eccentricities ($e > 0.8$). For very eccentric orbits, the projected amplitude of the stellar orbital motion can thus be up to a factor 2 or more smaller than the value calculated with Eq. 10. The variety of orbital arrangements reproduced by the set of planetary systems known to date does not

present any such case, as the eccentricity of the orbits is usually moderate ($e \leq 0.55$). The only exception is HD 160691 b ($e = 0.8$), but its astrometric signature ($\alpha = 139/\sin i \mu\text{as}$) is sufficiently high not to constitute a problem in terms of ability to detect it or to determine its orbit, even in the worst-case scenario.

In order to tackle the issues discussed in the previous Sections, we ran simulations of SIM narrow angle astrometric campaigns dedicated to the observations of the 11 stars known to harbor multiple-planet systems, utilizing the observing scenario sketched in Section 2.1. In particular, we generated sets of 500 planetary systems on the celestial sphere. The values we utilized for the stellar parameters and orbital elements were taken from various online catalogs in September 2002, as summarized in Table 1.⁶ The analysis carried out and results presented in this and the following Sections are based on a total of 990 000 simulated planetary systems.

Two orbital elements cannot be determined by radial velocity measurements, namely i and Ω . We simulate systems with random uniform distributions for the lines of nodes ($0^\circ \leq \Omega \leq 180^\circ$) and express detection probabilities as a function of the orbital inclination, constrained to vary in the range $1^\circ \leq i \leq 90^\circ$. Planet masses are scaled with the co-secant of the inclination angle.

An important point is the choice of the relative inclination angle between pairs of components in multiple systems. The relative inclination i_{rel} of two orbits is defined as the angle between the two orbital planes, and is given by the formula (see for example Kells et al. 1942):

$$\cos i_{\text{rel}} = \cos i_{\text{in}} \cos i_{\text{out}} + \sin i_{\text{in}} \sin i_{\text{out}} \cos(\Omega_{\text{out}} - \Omega_{\text{in}}), \quad (11)$$

where i_{in} and i_{out} , Ω_{in} and Ω_{out} are the inclinations and lines of nodes of the inner and outer planet, respectively. We choose the orbits of the multiple-planet systems shown in Table 1 to be perfectly coplanar, i.e. i and Ω are exactly identical for all the components in each systems. This choice has been adopted everywhere, unless otherwise noted.

There are three important questions related to the use of χ^2 statistics as a tool for multiple-planet detection that we aimed to answer:

- a) does detection probability depend on the shape and orientation of the orbits?⁷
- b) is detection of low signal-to-noise astrometric perturbations (the detection limit intrinsic to the χ^2 test is reached for $\alpha/\sigma_d \rightarrow 1$) influenced by the previous removal of larger astrometric signals?

⁶For an up-to-date list of extra-solar multiple-planet systems and their orbital elements as they are known at the time of writing see for example Fischer et al. (2003)

⁷In previous works (Lattanzi et al. 2000; S02) it was found that, for the case of single planets, averaging over orbital eccentricity, the astrometric detection probability based on the χ^2 test of the null hypothesis that the star is single did not depend upon the apparent orientation of the orbit

- 3) what is the behavior of false detections (once all planetary perturbations have been detected and removed) as a function of a broad range of orbital arrangements and astrometric signals?

Figure 1 shows, for each planet in each of the 11 systems considered, the results of the χ^2 test expressed as a function of the orbital inclination i . For each given system, the test was applied to the residuals to a single-star model, to a model containing the previously detected companion(s), and finally after the removal of all the Keplerian motions. In each system, the dominant signature is always easily detectable, regardless of the inclination of the orbital plane. Even long-period planets such as 55 Cnc d, due to its large mass, are unambiguously discovered. When the companion producing the larger signal is removed, the remaining components, due to the usually large astrometric perturbation induced on its parent star (even for edge-on configurations), are also detected without ambiguities, independent of the value of i , with the exception of the inner planet around HD 38529, the innermost planet orbiting ν And, and the middle planet in the 55 Cnc system.⁸ For the first two objects, in fact, in the edge-on configuration, the amplitude of the astrometric perturbation is of order of σ_d , thus the χ^2 test fails to recognize their presence about sixty percent of the time. 55 Cnc c has a minimum signature $\alpha \simeq 4 \mu\text{as}$, yet its detection probability in the edge-on configuration is a little below the 95% detection threshold due to the fact that its minimum mass also corresponds to the configuration in which only one dimension of the orbit is measurable by astrometry. As $i \rightarrow 0^\circ$, towards a face-on configuration, their projected masses increase, and in all cases detection probability reaches 100% for a value of $\sin i$ such that the correspondent astrometric signature $\alpha \simeq 2\sigma_d$. This result confirms what had been found in our previous works (Casertano et al. 1996; Casertano & Sozzetti 1999; Lattanzi et al. 2000; Sozzetti et al. 2001; S02). In particular, we find that, as long as the orbital period does not exceed the mission lifetime, detectability of astrometric perturbations close to the detection limit is not hampered by the presence of one or more companions producing larger signals. After the larger perturbations have been fitted and removed, a signal-to-noise ratio $\alpha/\sigma_d \simeq 2$ is sufficient for secure detection (at the 95% confidence level), just as if the planet was the only orbiting companion.

The last point addressed in Figure 1 concerns the fraction of false detections after all the planets have been discovered and removed. Due to the confidence level adopted for the χ^2 test, we expect $\sim 5\%$ of false positives if the subtraction of all planetary signatures has been successful. On the other hand, we may expect in principle that orbits with long or very short periods and producing low signal-to-noise ratios might not be accurately fitted and removed, with the result of larger spurious residuals, that could translate in a larger amount of false detections. As shown in Figure 1, the rate of false positives is roughly independent on the value of i , and comparable for all the systems investigated. Again, three exceptions are present, 55 Cnc c, HD 38529 b, and ν And b. In these three cases, the signal to be fitted approaches the detection limit as we move towards

⁸We recall that the astrometric signature $\alpha \propto T^{2/3}$, while the radial velocity amplitude $K \propto T^{-1/3}$, thus the *Hot Jupiters* on very short-period orbits, the first to be detected by spectroscopy, are most difficult to detect with the astrometric method

$i = 90^\circ$. The quality of the fits when $\alpha \simeq \sigma_d$ is poor, and this degradation translates into a number of false detections up to a factor 2 larger than the expected 5%, with a more pronounced trend as we move close to edge-on orbits. Instead, whenever all the planets in a given system produce a signal $\alpha > 2\sigma_d$ (even in the minimum mass configuration), then the number of false detections drops even below the expected threshold. We find that the average false detection rate, including all systems, is $\overline{F}_d = 3.2\%$, well within the predicted 5% of false positives in case of satisfactory removal of all planetary perturbations.

3.1.2. Periodogram Analysis

The χ^2 test only allows us to draw general conclusions on the need to reject or keep an a priori theoretical model describing the observations, but provides no clues to the actual nature of the residuals, if the assumed model is proven to be not consistent with the data. In order to provide a direct identification of the nature of the observation residuals and determine the true significance of planet detection/non-detection, a standard procedure is that of inspecting the data by means of a periodogram analysis, to search for evidence of the presence of a clear periodicity in the time-series.

At the end of each χ^2 test, we perform a periodogram analysis (utilizing the tools described in Section 2.2) to assess the presence or absence of further periodic signals. This test is applied to a set of observations that contain an a priori known set of planetary signatures, but nonetheless it has proven a useful exercise in order to gauge the ranges of applicability of this procedure to future, actual observations.

Table 2 shows a set of results pertaining to simulations of the 11 planetary systems assuming an average value of the common inclination angle ($i = 45^\circ$). The crucial points to be discussed are related to how well the period of the signal can be identified, and to how strong the signal must be with respect to the single-measurement precision, in order to give a peak z_p in the periodogram power allowing for a significant detection, i.e. a small value of the false-alarm probability. For the purpose of this analysis, we set a threshold $P(z_p) \leq 10^{-3}$, which implies, given the assumed number of independent frequencies discussed in Section 2.2, a value of $z_p \geq 12.0$ to ensure a significant detection of a periodic signal.

From inspection of Table 2, the first conclusion that can be drawn is that even in the case of an astrometric signal-to-noise ratio $\alpha/\sigma_d \simeq 1$, as long as the orbital period is shorter than the mission duration, a significant peak can be found in the spectrum. This is the case for example for HD 38529 b, that exhibits $\alpha/\sigma_d = 1.23$ (for $i = 45^\circ$), and while χ^2_ν approaches 1 (in fact, from Figure 1 its presence goes undetected about 15% of the time), the false alarm probability is well below the threshold, and the actual peak in the spectrum matches the true orbital period to within $\sim 1\%$. A graphical interpretation of the results for this system is given in Figure 2.

Secondly, three main period ranges can be identified, over which the efficacy of the periodogram analysis is significantly different. First of all, the orbital period may happen to be short enough

that the spectrum may peak at a value of T which departs significantly from the true one. This is for example the case of v And b, for which (see Figure 1) the probability of detection is close to 100% (in fact, $\alpha/\sigma_d = 1.64$, at $i = 45^\circ$), but the period is more than a factor 3 shorter than that of HD 38529 b, and the periodogram analysis fails to recognize the correct value of T , identifying a significant peak in the spectrum at a period value which is about an order of magnitude off the true one. As shown in Figure 3, bottom-left panel, only the second highest peak is close to the actual value of the period of v And b, but still about a factor 1.5 off. The failure of the periodogram analysis at very short periods can be dealt with at least in part in two ways. First of all, this problem may be corrected by increasing the number of observations. From the results in Table 2, in fact, we see how, in the case of randomly spaced data, it is possible to retrieve meaningful information on periods much shorter than the ‘average’ sampling rate in the case of evenly spaced data. For 24 two-dimensional observations distributed over 5 years, the average sampling rate would be ~ 0.2 yr, or 72 days. Due to the fact that *some* points are spaced much closer than that, the periodogram can effectively identify signals with periods as short as 15 days. Increasing the number of observations would obviously increase the ability to recover even shorter periods. Improvements in this direction can be obtained also by extending the range of test frequencies to values that are much greater than the average Nyquist frequency, and by over-sampling the spanned frequency range, in order to obtain information on frequency bins that are much smaller than the typically lowest independent frequency, that corresponds to the inverse of the timespan of the input data (i.e., the frequency such that the data can include one complete cycle). In our present analysis we have not quantified the effect of these different choices.

Furthermore, the results summarized in Table 2 tell us that well-sampled periods up to roughly the mission lifetime constitute ‘easy’ cases, for which the correct period can be identified with high confidence and accuracy (typically better than 7-8%), and this independently on the actual magnitude of the astrometric signature, as far as it lies above the single-measurement error. Figure 4 provides a graphical example of the results in Table 2 for the ‘easy’ case of HD 82943.

Finally, when $T > 5$ yr we enter a regime in which the classic periodogram is intrinsically doomed to fail. Increasing the number of observations (without increasing the mission length) or manipulating the frequency range and the way it is sampled does not improve the results. In fact, several authors (e.g., Black & Scargle 1982; Walker et al. 1995; Cumming et al. 1999) in the past highlighted that the periodogram power at periods exceeding the timespan of the data can be significantly reduced in the traditional periodogram formula. From the results in Table 2 we note how, in all the cases where the actual orbital period of the planet is greater than 5 years, the periodogram still identifies a significant periodic signal, but the peak systematically appears at a period of order of the total timespan of the data. Figure 5 provides a graphical representation of the data in Table 2 for the classic case of 55 Cnc, which harbors the planet with the longest period discovered so far. The situation is somewhat different from the spectroscopic case, where as T lengthens the radial velocity amplitude decreases, and indeed the peaks in the power spectrum relative to long period signals are significantly reduced. For astrometry, the amplitude of the

signal increases with increasing T , and in the sample of the presently known extra-solar planetary systems all companions are massive (as they are easier to detect by spectroscopy). The astrometric signal-to-noise ratio $\alpha/\sigma_d \gg 1$, and so, even if only a fraction of the orbit is sampled during the 5 years of simulated mission lifetime, the acceleration in the residuals is easily disentangled from the proper motion and a significant peak in the spectrum can also be identified. Nevertheless, the exact period cannot be recovered in a periodogram analysis. This systematic trend of a significant peak detected at $T \simeq L$ whenever the true period is greater than the timespan of the data is likely to become less evident for sufficiently small-mass planets (or, equivalently, sufficiently distant systems) on sufficiently long-period orbits. In fact, a reduction in the measured amplitude of long-period signals may occur either in the case of $\alpha/\sigma_d \rightarrow 1$ or when T is so long that secular effects such as proper motion begin overlapping efficiently to the astrometric signature. We have not investigated these issues here, as the main focus of this paper is on the actual characteristics of the multiple-planet systems discovered so far, and how they can be detected and measured with SIM.

3.1.3. Search for Periodicities when $T > L$

As we have seen, there exist regimes of orbital periods (shorter than the SIM mission lifetime) for which the Lomb-Scargle periodogram approach is robust, but others (comparable to or longer than the duration of the observations) for which the periodogram analysis fails to provide sensible results. One possible solution to overcome the ‘impasse’ was proposed in the recent past (Walker et al. 1995; Nelson & Angel 1998; Cumming et al. 1999). It consists of utilizing the zero point of the sinusoid in the fit as a free parameter, i.e. letting the mean of the data to float during the fit. This is contrary to what happens in the classic periodogram formula, in which the mean (taken as a proxy for the zero point) is subtracted from the data, and thus assumed to be perfectly known. When applied to radial velocity data, the floating mean periodogram approach has been shown to be successful at confirming existing companions and characterizing variations in the observation residuals due to long-period companions with orbits still awaiting phase closure (e.g., Fischer et al. 2001). We choose a different approach, with the aim of illustrating the potential of a strategy for period searches that tiles the classic periodogram approach to the Fourier analysis of periodic signals. When combined with the standard χ^2 statistics, this multi-method approach to planet detection provides an operational framework that may also be applied more in general to datasets from other astrometric observatories such as the upcoming ESA Cornerstone Mission GAIA (Perryman et al. 2001).

From the theory of Fourier analysis we know that a periodic, but non-sinusoidal, motion can be represented by a series containing a sinusoidal term at the fundamental frequency (corresponding to the actual period of the motion) plus higher order harmonics at exact multiple integers of this frequency, which carry on the information about the magnitude of the distortion from a purely sinusoidal motion due to the eccentricity (see for example Monet 1983). In the tangent plane to the celestial sphere, for the j -th planet in a system, the two components of its projected orbital

motion can then be written as:

$$\begin{aligned}
 x_{j,tan} &= \sum_{k=0}^{\infty} a_{k,j} \cos k\gamma_j t + \sum_{k=0}^{\infty} b_{k,j} \sin k\gamma_j t \\
 y_{j,tan} &= \sum_{k=0}^{\infty} c_{k,j} \cos k\gamma_j t + \sum_{k=0}^{\infty} d_{k,j} \sin k\gamma_j t
 \end{aligned}$$

where $j = 1, \dots, n_p$, and $\gamma_j = 2\pi/T_j$. The series is quickly convergent except for large eccentricities. For moderately eccentric orbits, say $e \leq 0.5$, three terms (fundamental, first and second harmonic) are sufficient to cover more than 95% of the signal (Jensen & Urych 1973; Konacki et al. 2002). For the purpose of our analysis, we have tested the ability of the above model to detect a significant long-period signal in the case of the five multiple systems (HD 37124, HD 38529, HD 74156, 55 Cnc, and 47 UMa) containing one planet on a moderately eccentric ($e \leq 0.40$), long-period orbit ($T > 5$ yr). We have limited the Fourier expansion to the second harmonic term ($k_{max} = 3$), and performed a linear fit (the unknowns being the parameters a_k, b_k, c_k, d_k , for $k = 0, \dots, k_{max}$) to the simulated SIM astrometric data relative to the systems described above, as a function of a large number of trial frequencies (4000) corresponding to the period range 0.01-20 yr. Under the assumption of coplanarity of the orbits, then in the case of 47 UMa the inner planet has a larger signature, thus the outer planet signal has been searched for utilizing a model in which the Fourier expansion is superposed to a fully Keplerian orbit for the inner planet. The results are summarized in Figure 6.

The two upper, the two middle, and the lower left panels show the behavior of the reduced chi-square χ^2_ν as a function of the dense grid of trial periods for the abovementioned systems, again setting an average value of the inclination $i = 45^\circ$. As opposed to the periodogram analysis, the Fourier series approach is capable of identifying the correct period of the outer planet, corresponding to the minimum of χ^2_ν , to better than 4% in all the five cases. The periodicity with the larger amplitude can be correctly retrieved with high accuracy independently of the underlying presence of the second, inner companion, which is clearly evident from the fact that χ^2_ν still departs significantly from unity even at its minimum. There are two exceptions, i.e. 47 UMa c, beyond which at present no other planetary companions have been discovered, and HD 38529 b, for which χ^2_ν appears to be consistent with the outer planet being the only one in the system due to the very low signature induced by the inner planet. Nonetheless, as we have seen in the previous Section, the signal from the inner companion can still be identified in the periodogram power spectrum with high confidence, even in a case in which the χ^2 statistics approach is more sensitive to failure. These results underline the importance of utilizing a range of different tools for planet detection, which can be combined in order to improve significantly the efficiency with which planetary signatures can be revealed even at low values of the astrometric signal-to-noise ratio α/σ_d .

Finally, we note how in Figure 6 the minima of χ^2_ν for HD 37124 c, 55 Cnc d, and 47 UMa c are broader than those for HD 74156 c and HD 38529 d. This is primarily due to the combined effect of the magnitude of the astrometric signature induced on the parent star and the fraction of the orbit

covered by the observations. For comparison, the lower right panel shows the results of a simulation in which the same fitting procedure was applied to our own solar system (nine independent, coplanar Keplerian orbits), placed at different distances from the observer. The dominant signature is the one associated with Jupiter, and its period is easily identified with an accuracy of 5-6%. As we move farther away from the observer, the value of the minimum of χ_ν^2 , which is initially located at $\chi_\nu^2(\min) = 1.26$, indicating the presence of a second underlying signal (from Saturn, the second heaviest planet in our system and the one producing the second largest signature), decreases, and eventually at 10 pc it is perfectly consistent with Jupiter being the only planet around the Sun. At the same time, while the presence of the second largest planet becomes undetectable, also the signature from Jupiter decreases and correspondingly, for the same fraction of the orbit covered by the observations, the slope of the χ_ν^2 curve at long periods becomes increasingly less steep.

In the perspective of the optimization of a global search strategy for the determination of the best configuration of starting values for the orbital parameters in the fully Keplerian fit *for newly discovered planetary mass objects*, a precise guess for the actual value of the orbital period is needed, in order to try to minimize the dimensions of the parametric space to be searched. Suppose in fact we select as plausible preliminary values of T those whose χ_ν^2 difference with the minimum $\chi_{\nu,\min}^2$ is less than 15% of the latter value, as done by Guirado et al. (1997) in their astrometric orbit determination of a low-mass companion around the star AB Doradus. This would mean that, for the cases shown in Figure 6, assuming no spectroscopic orbits are available, plausible starting guesses for the orbital period in a subsequent global least-squares fit would lie in the ranges reported in Table 3. As it is clear, whenever we have a configuration approaching a regime in which χ_ν^2 has a very broad minimum (HD 37124 c, 47 UMa c, 55 Cnc d, Jupiter at 10 pc), this corresponds to a range of plausible starting guesses for the period covering several years, and it is likely this would cause accurate orbit determination and mass measurements to become a more difficult task.

Clearly, the results shown in these Sections constitute only a very preliminary investigation of the potential of the approach to the problem of real-life detection of *newly discovered planetary systems* with a method that combines χ^2 statistics, periodogram and Fourier analysis of SIM astrometric observation residuals. Due to the illustrative purpose of our work, some important topics have been left aside, such as estimates of the degradation in SIM’s ability to detect planets with low values of α/σ_d on long-period orbits due to significant correlation with the target’s proper motion. Also, some relevant technical issues remain open, such as the possibility to not only provide robust estimates of the reliability of the adopted model, through additional statistical hypothesis testing (e.g., Bevington & Robinson 2003), but also assess the reliability of the estimates themselves, through further testing and placing statistical constraints on the post-fit observation residuals and their covariance matrices, in order to select the optimal least-squares solution (e.g., Bard 1974; Bernstein 1997). Nevertheless, within the limited scope of our study, we have been able to provide quantitative examples which are useful for understanding that it will be very beneficial if a variety of numerical and statistical tools will be implemented to maximize the robustness of the method aimed at verifying the true significance and reliability of a detection.

3.2. Multiple-Planet Orbits Reconstruction

Once a reliable detection of a system of planets has been established, a number of other important issues must be addressed, all primarily related to how well it is possible to measure the orbital parameters and masses of each planet.

As soon as the number of planets in a system is greater than one, the parameter space to investigate becomes immediately very large. In this illustrative study, we have parameterized the ability of SIM to measure multiple-planet systems in terms of their astrometric signatures, orbital periods, eccentricities, and inclinations of the orbital planes. We have then investigated the potential of SIM to make meaningful coplanarity measurements by gauging how accurately the relative inclination of pairs of planetary orbits may be determined. Finally, we have quantified the improvement in the accuracy on the determination of orbital parameters and masses that maybe reached when both astrometric and spectroscopic data are available.

3.2.1. Accuracy in Orbit and Mass Determination

The first relevant question to be addressed is: what is the impact on the accuracy in orbital parameters and mass determination when the number of planets in a system is larger than one, and the number of parameters to be fitted correspondingly increases?

Table 4 shows, for each planet in the 11 systems under consideration, the ratios of rms errors σ_m for the most relevant parameters (M_p , a , T , e , and i) derived from a multiple-planet fit to the same quantities σ_s obtained from a single-planet solution (in simulations where only one planet was generated around the observed parent star). The values are averaged over the inclination angle.

In general, for planets with periods $T \leq L$, the two-planet fit (or three-planet fit, as in the case of v And and 55 Cnc) degrades the orbital elements and mass estimates by $\sim 30 - 40$ % with respect to the single-planet fit, with typical fluctuations of order of $5 - 10$ % among different parameters. From closer inspection of Table 4, some particularly interesting cases stand out.

First of all, there is a clear trend for larger values of the ratio σ_m/σ_s for a given parameter, as the magnitude of the astrometric signature decreases. For example, HD 82943 b and HD 82943 c, with signatures of only $65/\sin i \mu\text{as}$ and $22/\sin i \mu\text{as}$ respectively (see Table 1), have values of the rms errors typically about a factor 2 or more larger than the respective single-planet case, as opposed for example to the case of the Gliese 876 system, in which the two planets, producing larger signals, are measured together only about 20% worse than if they were the only orbiting bodies.

The second relevant feature arising from the results of Table 4 concerns those systems in which the orbit of the outer planet is not fully sampled during the 5 years of simulated SIM observation. In three such cases (HD 38529 c, HD 37124 c, and HD 168443 c), the ratios $\sigma_m/\sigma_s \leq 1$ for almost

all parameters shown in Table 4. The reason for this is to be found in the intrinsic superiority of the model containing more than one planet, when it is applied to configurations where the outer planet has $T > L$ and produces a signature much larger than the inner one. In fact, the larger number of free parameters (with respect to the single-planet case) is compensated by the superior model, and the net result is that in the least squares solution a smaller fraction of the outer planet’s signal is identified as proper motion, with the consequence of a more precise determination of the outer planets’ orbital elements and masses as opposed to the single-planet solution (up to about a factor 2-3 better). This behavior is not very prominent for 55 Cnc d, due to its much longer period ($T \simeq 3L$), which translates in such poor sampling of the orbit that the larger signature is not enough for the orbital solution to improve significantly.

Finally, the case of the 47 UMa system stands out. Assuming coplanarity of the two planets’ orbits, then the astrometric signature of the outer one is smaller. The inner planet’s orbit is sampled completely only once during the timespan of SIM observations, and the outer planet’s period is 1.42 times longer. Even utilizing the spectroscopic orbital elements as starting guesses for the iterative least square procedure, the net result is that a significant portion of the inner planet’s signal is assigned to the outer one, and the accuracy in the determination of semi-major axis, period, and mass is degraded by over an order of magnitude with respect to the single-planet solution. For what concerns the uncertainties on eccentricity and inclination angle, the degradation effects due to this particular configuration are only marginal. However, the orbital solution for the outer planet does not benefit from this redistribution of the inner planet’s signal, and its orbital parameters and mass are also more poorly determined than in the single-planet case.

In Figure 7 and 8 we provide a detailed visualization of the results on orbit reconstruction and planet mass determination for the three-planet system 55 Cnc and the two-planet system HD 12661, which are representative of the variety of configurations addressed in this study, i.e. well-sampled, well-spaced orbits, or poorly sampled due to either very short or very long periods, high values of the astrometric signal-to-noise ratio as well as values of α/σ_d approaching 1. In the two Figures, the fractional deviation of the measured from the true value for the five relevant parameters discussed above is plotted against the inclination angle, both in the case of single- and multiple-planet realizations. Four of the five parameters (M_p , a , e , and i) are primarily sensitive to the value of α/σ_d . The larger the astrometric signal-to-noise ratio, the more accurate their measured value, independently on the orbital period. So for example in the 55 Cnc system the outermost planet has these parameters best measured (even though only one third of its orbit is sampled), while the middle planet’s parameters are the least accurately determined. An important exception in this case is the orbital eccentricity of the innermost planet: its orbit is tidally circularized ($e = 0.02$), and although its astrometric signature is a factor 2 larger than the middle planet, its period is so short that the inadequate sampling causes the value of e to be more poorly constrained as compared to the one of the middle planet. On the contrary, the accuracy with which T itself is retrieved primarily depends on how well the orbit is sampled (center left panels in Figures 7 and 8). Thus, wider orbits have the period less accurately measured, while the accuracy on the determination of

the other parameters is improved.

As the inclination i decreases, we move from a perfectly edge-on to almost face-on configuration, i.e. from a situation in which only one dimension is actually measured to one in which the SIM measurements provide full two-dimensional information. At the same time, the true mass inferred for each planet from the radial velocity data increases, therefore the astrometric signature is larger. These effects combined translate into increasingly more accurate measurements of the planet’s mass, semi-major axis, eccentricity, and period, as $i \rightarrow 0^\circ$. At the same time, the observations are less sensitive to the inclination itself, and its fractional measurement error increases (lower left panels in both Figure 7 and 8).

The present set of extra-solar planetary systems covers a relatively wide range of shapes and sizes of the orbits, and planetary masses. We can then attempt to generalize the results presented here to characterize the variety of configurations of potential planetary systems in the solar neighborhood for which SIM could provide accurate measurements, for the given template observing strategy outlined in Section 2.1. In the three-dimensional parameter space defined by astrometric signal-to-noise ratio α/σ_d , period T , and eccentricity e we have identified the loci for the measurement of a given orbital parameter or mass of a planet in a multiple system to a specified level of accuracy. Figure 9 shows iso-accuracy contours for M_p , a , T , e , i , and Ω (expressed in percentages of the true value) in the $e - T$ plane. The results are averaged over the inclination angle. The general indication is that the correlation between these two parameters is relatively limited. When the sampling is poor due to very short-period orbits, the degradation in accuracy is common to all parameters, and regardless of the orbital eccentricity. For well-sampled orbits, the parameters can be measured better, with varying degrees of improved accuracy. Again, the results are essentially insensitive to e . In fact, massive planets on relatively long-period orbits such as 55 Cnc d produce astrometric signals large enough that the fraction of the orbit covered by the observations still allows for accurate measurements of the orbital elements, regardless of the value of the eccentricity. An important exception is constituted by the accuracy on the eccentricity itself (central right panel), which appears to degrade for periods exceeding the 5-year SIM mission duration, unless $e \geq 0.1$.⁹ Finally, it must be noted how the accuracy in the determination of the orbital period (central left panel) shows a behavior opposite to that of the other parameters, in agreement with the fact that how well the periodicity of the astrometric signal can be measured depends upon the number of times an orbit is fully sampled. The same mostly uncorrelated behavior is evident in the plane defined by signal-to-noise ratio and eccentricity.

Figure 10 shows the same results, but this time in the plane defined by α/σ_d and T . Here we appreciate a clear correlation between these two crucial parameters, as it is shown by the trend

⁹When the orbital period is sufficiently long or the mass of the planet sufficiently low, instead, e is likely to play an important role in the degradation of the reachable accuracy on other parameters as well, as eccentric orbits not sampled in correspondence of the pericenter passage may not be properly measured by the fitting algorithms due to a lack of curvature sufficient to disentangle the periodic motion from the stellar proper motion

for lower accuracy on M_p , a , e , i , and Ω towards low values of α/σ_d and short periods, and for improved determination of orbital elements and masses for large values of α/σ_d and longer periods. Again, the orbital period itself behaves in an opposite fashion.

It is possible to provide an analytic representation for the dependence of the fractional errors on the estimated orbital elements and masses as a function of the three quantities α/σ_d , T , and e . In order to do so, we have performed a fit to the data (i.e., the fractional uncertainties σ_p on a given parameter, where the subscript p can be equal to M_p , a , T , e , i , or Ω) with a model of the form:

$$\sigma_p(\%) = \eta_0 \times (\alpha/\sigma_d)^{\eta_1} \times T^{\eta_2} \times e^{\eta_3} \quad (12)$$

The results are summarized in Table 5, and are averaged over the inclination angle. Again, similarly to what we saw in Figures 9 and 10, we realize how, for example, the fractional errors on M_p , a , and i are dominated by the behavior of α/σ_d and T , while the dependence on e in such cases is relatively weak. For σ_e , instead, the dependence on the eccentricity itself is much stronger. Finally, in the case of σ_T , the exponent of α/σ_d , that would have the fractional error on the orbital period decrease as the astrometric signal-to-noise ratio increases, is largely compensated by the opposite, and stronger, dependence on T itself, with the result that, as T increases, σ_T grows larger as well. It is important to stress the limits of applicability of such empirical multi-dimensional power-laws. In fact, these formulas do not include a variety of effects, such as the degradation induced by the increasingly poor sampling at very short or very long periods. Due to the former effect, for example, the best-fit formula for σ_T systematically underestimates the errors on the orbital period for $T < 0.1$ yr. In general, the agreement between the power-laws shown in Table 5 and the data is good when the values of σ_p are larger than 1%, while discrepancy factors of a few typically arise when the fractional errors on the parameters become very small. Finally, we expect the functional dependence of the fractional errors on α/σ_d , T , and e , as well as the values of the zero-points η_0 , to be somewhat different when a range of possible observing strategies and different values of the measurement errors were to be considered. In our exploratory work we have not investigated further such issues.

Taking into account the results reported in Tables 4 and 5 and those summarized in Figures 9 and 10, we can attempt to draw some general conclusions as for what concerns the ability of SIM to measure the most relevant parameters in multiple-planet systems: on average, 10% accuracy, or better, will be reached in the determination of the mass of planets in two or three-planet systems with components on periods not shorter than $T \simeq 0.1$ yr, and producing an astrometric signal-to-noise ratio $\alpha/\sigma_d \geq 5$. Similar accuracy will be attainable for systems containing massive planets with periods longer than the SIM mission duration (up to $T \simeq 3L$), which produce $\alpha/\sigma_d \geq 100$. The semi-major axis, orbital inclination, and lines of nodes will behave similarly, while the eccentricity will require $\alpha/\sigma_d \simeq 10$ for periods $T \leq L$, and accurate measurements will become increasingly more difficult to achieve for periods exceeding the mission lifetime. The orbital period will be recovered with typical accuracies of a fraction of a percent for $T \leq L$. Even for objects with $T \simeq 3L$ and producing $\alpha/\sigma_d \gg 1$, such as 55 Cnc d, 1% accuracy should be attainable.

3.2.2. Coplanarity Measurements

As discussed in the Introduction, the increasing number of extra-solar planetary systems has motivated detailed theoretical studies on their dynamical evolution and long-term stability. It is worth mentioning in detail the main results derived so far for some of the systems which have been the target of the larger theoretical efforts. For example, in the case of the ν And system, neglecting to first order the effects of the innermost planet on the overall stability of the system, Stepinski et al. (2000) come to the conclusion that dynamical stability requires the orbital inclination of the outer two companions to be greater than $i \sim 13^\circ$, otherwise the two objects would be too massive and gravitational interactions would disrupt the system. Furthermore, the system cannot be stable in the long term if relative inclinations are greater than 55° , 35° , and 10° , for $i \sim 64^\circ$, $i \sim 30^\circ$, and $i \sim 15^\circ$, respectively: then, the more massive the planets, the closer to coplanarity their orbits have to be, for the system not to be destabilized on a short time-scale. As for what concerns the strongly interacting two-planet system on short-period orbits around Gliese 876, Laughlin & Chambers (2001), Rivera & Lissauer (2001b), and Goździewski et al. (2002) have found limits for dynamical stability on their relative inclinations that, similarly to the ν And case, are a strong function of the unknown inclination of the orbital planes (and thus unknown masses): the relative inclinations of stable systems can vary in the ranges of $\pm 15^\circ$ for $\sin i = 0.5$ up to $\pm 90^\circ$ for $\sin i = 1$. Finally, Laughlin et al. (2002) have studied extensively the 47 UMa system, and found that, somewhat surprisingly, the mutual inclination of the two long-period planets orbiting 47 UMa must be less than 45° for the system to be stable, but the results are essentially insensitive to the actual planet masses.

As the above results clearly suggest, dynamical limitations on the relative inclinations and masses of planetary companions in extra-solar multiple-planet systems cannot be stated very precisely. Such estimates suffer from large uncertainties due to the typically poorly constrained orbital inclinations and planet masses, and undetermined position angles of the lines of nodes. More accurate observational data to complement the one-dimensional radial velocity measurements are needed before the details of the long-term evolution of multiple-planet systems can be assessed with a high degree of confidence.

Figure 11 shows the estimated accuracy with which SIM would measure the coplanarity of the orbits of the present set of extra-solar planetary systems. After the multiple-planet fit, the estimated values of i and Ω for all components in each system were used to derive their actual relative inclination (Eq. 11). In Figure 11, for each system, the relative inclination of each pair of planets is plotted against the (common) inclination of the orbital plane with respect to the plane of the sky. The corresponding error bars have been computed by propagating (Eq. 9) the formal expressions from the covariance matrix of the multiple-planet fit.

In order to establish coplanarity, we must measure $i_{\text{rel}} \simeq 0^\circ$. The first seven panels show how, as long as all components in a given system have minimum masses and orbital periods such that the astrometric signal-to-noise ratio is favorable ($\alpha/\sigma_d \simeq 10$ or greater) for any inclination

of the orbital plane with respect to the plane of the sky, the quasi-coplanarity of each pair of planetary orbits can be assessed with high accuracy. Even in the case of two systems with one of the planets having period exceeding the timespan of the observations (HD 37124 and 47 UMa), the net result is that for such well-measured systems the relative inclination can be determined to be $i_{\text{rel}} \leq 3^\circ$, with relative uncertainties of a few degrees. The next seven panels of Figure 11 highlight instead how, when dealing with astrometric signatures approaching the detection limit ($\alpha/\sigma_d \rightarrow 1$), to make accurate coplanarity measurements will be a significantly more challenging task. In the specific cases shown, only towards quasi-face-on configurations, in which the signal from the smaller and/or shorter period planet becomes large enough (due to significantly larger projected mass), the results resemble those obtained in the favorable cases. Otherwise, the relative inclinations will typically be measured to be $i_{\text{rel}} \sim 10^\circ$ or greater, with uncertainties of additional tens of degrees. Finally, as the bottom right panel shows, for the two outer planets of the ν And system quasi-coplanarity can be reliably established, in agreement with the findings of Sozzetti et al. (2001).

It is worth mentioning another interesting feature arising from the results presented in Figure 11. Almost all panels show a more or less pronounced trend for increasing uncertainties in the determination of i_{rel} as we move away from the edge-on configuration, with a somewhat sharp change in behavior as $i \rightarrow 0^\circ$. The explanation is to be found in the details of the dependence of i_{rel} on i_{in} , i_{out} , and the difference $\Omega_{\text{out}} - \Omega_{\text{in}}$. In fact, as i decreases, the uncertainty in the position angle of the line of nodes grows, because of the increasing difficulty in its correct identification (Ω eventually becomes undefined at $i = 0^\circ$). However, the uncertainty in the value of i_{rel} defined in Eq. 11 increases correspondingly only up to the point in which, for sufficiently low values ($i \leq 5^\circ$) of the inclination angles, the second term $\sin i_{\text{in}} \sin i_{\text{out}} \cos(\Omega_{\text{out}} - \Omega_{\text{in}})$ of the right-hand side becomes essentially negligible with respect to the first term $\cos i_{\text{in}} \cos i_{\text{out}}$, irrespective of the fact that the uncertainty of the line of nodes keeps on growing. Thus, ultimately for quasi-face-on configurations an accurate knowledge of Ω_{in} and Ω_{out} is not required. In their recent work on extra-solar planetary system detection and measurement with GAIA, Sozzetti et al. (2001) do not consider orbital configurations of the ν And system with inclination angles less than 5 degrees. As a consequence, they come to the conclusion that when $i \rightarrow 0^\circ$ accurately estimating the coplanarity of the outer two planets of the ν And system would be difficult because of the increasing uncertainties on the measurement of Ω for the two planets. Here instead we have shown how the relative inclination becomes essentially insensitive to the retrieved values of Ω_{in} and Ω_{out} , as we approach a perfectly face-on configuration.

Finally, simulations of non-coplanar systems with $\Omega_{\text{in}} \neq \Omega_{\text{out}}$ and/or $i_{\text{in}} \neq i_{\text{out}}$ yielded similar results. Our findings help to reaffirm the importance of SIM high-precision position measurements in verifying the stability of multiple-planet system. Accurately determining the inclination angles and lines of nodes of multiple planetary orbits will allow in turn to derive meaningful mass and relative inclination angle estimates, which will be used to better constrain the results from theoretical studies on the long-term evolution of planetary systems.

3.2.3. Combining Radial Velocity and Astrometric Data

In recent works, Eisner & Kulkarni (2001a, 2001b, 2002) have utilized a semi-analytical method to show how planet detection efficiency would benefit from the simultaneous availability of both astrometric *and* radial velocity measurements, especially as far as long-period, edge-on orbits are concerned. This combined approach has indeed proved very successful when dealing with real data. For example, utilizing both astrometric measurements from the Fine Guidance Sensor 3 on board the *Hubble Space Telescope* and ground-based precision radial velocity data, Benedict et al. (2001) have improved the accuracy on the mass estimates for the M dwarf binary Wolf 1062 by a factor 4 with respect to the same values obtained by Franz et al. (1998) using only *HST* astrometry. Very recently, the same combined method revealed itself an essential ingredient in the spectacular determination of the first actual mass of an extra-solar planet, the outer component in the Gliese 876 system (Benedict et al. 2002).

Usually, a combined astrometric + spectroscopic orbit is obtained by modeling time-series of data from both techniques in a simultaneous least-squares solution, with a few additional constraints, the most important of which is the identity (Pourbaix & Jorissen 2000):

$$\frac{\alpha \sin i}{\pi_{\star}} = \frac{TK_1\sqrt{1-e^2}}{2\pi \times 4.7405}, \quad (13)$$

which relates quantities only derived from astrometry (inclination angle, astrometric signature, and stellar parallax on the left-hand side) to quantities derivable from both techniques or radial velocity alone (orbital period and eccentricity, and radial velocity semi-amplitude of the primary on right-hand side).

In our exploratory work, we have adopted a more limited approach. For each of the 11 planetary systems under study, we have utilized the orbital elements derived from spectroscopy (T , e , τ , and ω) as constraints in the sense that we have kept them fixed to their input values in the global least-squares iterative solution, and solved only for α , i , Ω . Figure 12 shows the estimated improvement that may be obtained in the determination of planet mass, semi-major axis, and inclination when SIM relative astrometry of the presently known planetary systems is “combined” (in the abovementioned sense) with spectroscopy, as opposed to the scenario in which all orbital elements are solved for in the least-squares minimization procedure. The three contour plots identify, in the plane defined by α/σ_d and T , regions of increasingly larger values of the ratio σ_G/σ_C between the estimated fractional uncertainties on M_p , a , and i in the case of ‘global’ orbital fits in which all parameters were adjusted and the same quantities as computed after the ‘constrained’ fits. The results are averaged over the inclination angle.

The general indication is that for well-sampled orbits, with large astrometric signatures the constrained fit does not improve significantly the final accuracy of the results. In such cases, typically $1 \leq \sigma_G/\sigma_C \leq 2$. The ability to recover accurate values of M_p , a , and i will be improved especially when the period is larger than the timespan of the observations (and the astrometric signal-to-noise ratio is very large), with typical values of $\sigma_G/\sigma_C \geq 6$ for a and M_p , while the

inclination is less sensitive to the constrained solution. For low values of α/σ_d and short-period orbits the improvement on the fractional accuracy for the fitted parameters will be marginal.

In their work on multiple-planet system detection and measurement with GAIA, Sozzetti et al. (2001) suggested that, for systems with configurations very close to face-on, the accuracy of the inclination measurement will be substantially increased by combining radial velocity and astrometric data. On the other hand, although in their work they focused mainly on combining astrometry and radial velocity in the case of edge-on (single-planet) orbits, Eisner and Kulkarni (2002) argue that the short-period accuracy of astrometry + radial velocity should be approximately independent of orbital inclination. In Figure 13 and 14 we show the behavior of the ratios σ_G/σ_C for M_p (upper panels), a (central panels), and i (lower panels) as a function of the common inclination of the orbital plane for four representative systems (55 Cnc, 47 UMa, HD 12661, and HD 38529), whose characteristics allow us to provide quantitative answers to the above arguments. Although the predictions made by Sozzetti et al. (2001) and Eisner & Kulkarni (2002) are in general confirmed, when it comes to multiple-planet orbital fits some details become more subtle and complex. In fact, not only the average value of the ratios σ_G/σ_C (as shown in Figure 12), but also their behavior as a function of the orbital inclination depends on the ranges of periods and astrometric signatures we are dealing with. In the case of 55 Cnc d, for example, with a period $T \simeq 3L$, the accuracy on all fitted parameters benefits greatly from a constrained fit, which minimizes the residual covariance between the orbital solution and the solution for the parallax and the proper motion of the primary. The improvement in orbit reconstruction reaches its maximum for an almost face-on configuration. On the other hand, for 47 UMa c and HD 38529 c, with $T \simeq 1.4L$ and $T \simeq 1.2L$ respectively, σ_G/σ_C increases as $i \rightarrow 0^\circ$ only in the case of i itself, while the semi-major axis is almost insensitive to the inclination angle. In the range of periods $T < L$, again different parameters behave slightly differently, in these cases primarily due to the magnitude of α/σ_d . While the accuracy on orbital inclination is only marginally improved towards face-on configurations, the estimated semi-major axis (and in turn the derived planet mass) is more accurately retrieved in a constrained fit on an edge-on configuration, in which case astrometry loses completely the second dimension of the measurements.¹⁰ For an accurate determination of the semi-major axis, the combination between astrometric and spectroscopic data will be effective particularly when $\alpha/\sigma_d \rightarrow 1$, as in the case of HD 38529 b or 55 Cnc c, while for example the results for the two planets in the HD 12661 system, both with large signatures, are only marginally improved by the constrained fit.

¹⁰A noticeable exception is constituted by 47 UMa b, that exhibits significant improvement in the accuracy with which its semi-major axis can be determined when the configuration is face-on. This behavior is due to the particular orbital arrangement of the system, with the longer period planet producing the smaller astrometric signal, under the assumption of coplanar orbits

4. Summary and Conclusions

The properties of extra-solar giant planets detected by radial velocity surveys of nearby solar-type stars (Marcy et al. 2002a) seem to indicate that the Solar System configuration is just one of the many possible outcomes of disk evolution around young stars. Indeed, the strong coupling between the early evolutionary processes of a star and its disk can have a significant impact on planet formation time-scales and the final orbital configurations after the disk dissipates.

Over the next decade or so, a series of new instruments will come on line, which will provide data of great value to shed new light in the complex scenarios of the formation and evolution of planetary systems. Among indirect detection techniques, ground-based precision spectroscopy, the most successful technique so far, will be complemented by high-precision ground-based (Keck Interferometer, VLTI) and space-borne (SIM, GAIA) astrometry, and transit photometry from ground (e.g., OGLE III, STARE, STEPSS, Vulcan Camera Project) and in space (Corot, Kepler, Eddington). In the field of direct detection techniques, near- and far-infra-red diffraction-limited ground- and space-based imaging (ALMA, SIRTf, JWST) will pave the way to ambitious projects of coronagraphic/interferometric imaging from space (TPF, Darwin), with the long-term goal of directly imaging terrestrial planets in the Habitable Zone of nearby stars.

In this paper we have completed the analysis begun in our previous works (Casertano & Sozzetti 1999; S02), in order to connect and relate the basic capabilities of the Space Interferometry Mission (SIM) to the properties of extra-solar planetary systems. We have utilized detailed end-to-end numerical simulations of sample SIM narrow-angle astrometric observing campaigns (Section 2.1), an improved methodology for planet detection which combines χ^2 statistics, periodogram analysis, and Fourier series expansions (Sections 2.2), an upgraded analytical model that allows for multiple-planet orbital fits (Sections 2.3), and the set of presently known extra-solar planetary systems as templates. The experiments described in this paper have allowed us to quantify the limiting capability of SIM to discover systems of planets around solar-type stars in the solar neighborhood (Sections 3.1.1, 3.1.2, and 3.1.3), measure their orbital properties and masses (Sections 3.2.1 and 3.2.3), and accurately determine the coplanarity of multiple-planet orbits (Section 3.2.2). Our main results can be summarized as follows.

1. Additional planets in systems have little impact on SIM ability to detect each component in a system, in comparison to the single-planet configurations. The inaccurate fit and subtraction of orbits with astrometric signal-to-noise ratio $\alpha/\sigma_d \rightarrow 1$ can on the other hand increase the false detection rate by up to a factor 2. The periodogram analysis adds robustness to the detection method when $T \leq L$, by singling out periodicities even in the case of α/σ_d close to the χ^2 detection limit. For very short-period orbits, a more dense time-series of observations will be the obvious choice in order to overcome poor sampling. When $T \geq L$, the least squares technique combined with Fourier analysis can correctly identify periods as long as three times the timespan of the observations. This approach is arguably preferable, as opposed to the periodogram method, which needs modifications in the long-period regime.

2. Accurate measurements of multiple-planet orbits and determination of planet masses are only moderately affected by the presence of more than one object in a system, with typical degradation of 30-40% with respect to single-planet solutions. When $T \leq L$, it is possible to determine masses and orbital inclinations to better than 10% for systems with planets having periods as short as 0.1 yr, and for systems with components producing astrometric signals as low as $\sim 5 \sigma_d$, while $\alpha/\sigma_d \simeq 100$ is required in order to measure with similar accuracy objects with periods as long as three times the mission duration. Orbital eccentricity typically requires larger signals for the same accuracy level, and its correct identification can become a non trivial task when $T \geq L$. The accuracy on estimated orbital elements improves significantly as we move towards face-on orbits, except for the inclination angle.
3. Accurate coplanarity measurements are possible for systems with all components producing $\alpha/\sigma_d \simeq 10$ or greater. In the case of truly coplanar systems, the relative inclination between pairs of planetary orbits is measured to be $i_{\text{rel}} \leq 3^\circ$, with uncertainties of a few degrees, for periods $0.1 \leq T \leq 15$ yr. In systems where at least one component has $\alpha/\sigma_d \rightarrow 1$, uncertainties on i_{rel} of order of $30^\circ - 40^\circ$, or larger, are likely to preclude a robust assessment of the system coplanarity.
4. Whenever feasible, an approach that combines astrometry and radial velocity will yield significantly more accurate estimates of planet masses and orbital elements. The uncertainties on orbital elements and masses can be reduced by up to an order of magnitude, especially in the case of long-period orbits in face-on configurations, and for low amplitude orbits seen edge-on. Well-sampled, well-measured orbits ($T \leq L$, $\alpha/\sigma_d \gg 1$) are only marginally affected by the combination of astrometric and radial velocity measurements.

Our results reaffirm the important role future high-precision space-borne astrometric missions promise to play in the realm of extra-solar planets. With its unprecedented astrometric precision, SIM will not only complement other on-going and planned spectroscopic, astrometric, and photometric surveys, but its position measurements will have a unique impact in the study of some important aspects of multiple-planet systems. By directly measuring the line of nodes and inclination angle for each component in a system, SIM will determine whether planetary orbits are coplanar with uncertainties of a few degrees. For instance, this will provide theory with the observational evidence needed to address the long-term evolution issue, and draw sensible conclusions on the chaotic and stable/unstable dynamical behavior of multiple-planet orbits. The same SIM measurements will also be instrumental to help confirm or rule out one of paradigms which form the basis for present-day theoretical models, i.e. that the sole conceivable environment for planet formation are flattened circumstellar disks around young pre-main sequence stars. If multiple-planet orbits are found to be coplanar, this will indicate that planetary systems indeed originate and evolve in a way similar to our own (Lissauer 1993; Pollack et al. 1996). If large relative orbital inclinations were found, this would provide evidence that other systems are truly different from ours, and thus their present configurations should be explained in terms of either an early, chaotic

phase of orbital evolution or formation by another mechanism such as disk instability (Boss 2000, 2001; Mayer et al. 2002).

This project was partially funded by the Italian Space Agency under contract ASI-I/R/117/01 (to A. S. and M. G. L.). We thank an anonymous referee for a very careful reading of the paper and for illuminating comments that helped improve the original manuscript. A. S. is greatly indebted to the Smithsonian Astrophysical Observatory and its Computation Facility for kind hospitality and technical support during the completion of this work. This research has made use of the SIMBAD database, operated at CDS, Strasbourg, France.

REFERENCES

- Artymowicz, P. 2001, BAAS, 33, #10.01
- Bard, Y. 1974, *Nonlinear Parameter Estimation*, New York: Academic Press
- Barnes, R., Quinn, T. 2001, ApJ, 550, 884
- Benedict, G. F., et al. 2001, AJ, 121, 1607
- Benedict, G. F., et al. 2002, ApJ, 581, L115
- Bernstein, H.-H. 1997, Proc. ESA Symp., Hipparcos - Venice '97, ESA SP-402, 705
- Bevington, P. R., Robinson, D. K. 2003, *Data reduction and Error Analysis for the Physical Sciences* - 3rd ed., Boston: McGraw-Hill
- Black, D. C., Scargle, J. D. 1982, ApJ, 263, 854
- Booth, A. J., et al. 1999, in *Working on the Fringe: Optical and IR Interferometry from Ground and Space*, ed. S. Unwin & R. Stachnik, ASP Conf. Series, 194, 256
- Boss, A. P. 2000, ApJ, 536, L101
- Boss, A. P. 2001, ApJ, 563, 367
- Butler, R. P., et al. 1999, ApJ, 526, 916
- Butler, R. P., Marcy, G. W., Vogt, S. S., Fischer, D. A., Henry, G. W., Laughlin G., Wright, J. 2003, ApJ, 582, 455
- Casertano, S., Lattanzi, M. G., Perryman, M. A. C., Spagna, A. 1996, Ap&SS, 241, 89
- Casertano, S., Sozzetti, A. 1999, in *Working on the Fringe: Optical and IR Interferometry from Ground and Space*, ed. S. Unwin & R. Stachnik, ASP Conf. Series 194, 171
- Charbonneau, D., Brown, T. M., Latham, D. W., Mayor, M. 2000, ApJ, 529, L45
- Charbonneau, D., Brown, T. M., Noyes, R. W., Gilliland, R. L. 2002, ApJ, 568, 377
- Chiang, E. I., Tabachnik, S., Tremaine, S. 2001, AJ, 122, 1607
- Chiang, E. I., Murray, N. 2002, ApJ, 576, 473
- Colavita, M. M., et al. 1999, ApJ, 510, 505
- Cumming, A., Marcy, G. W., Butler, R. P. 1999, ApJ, 526, 890
- Cuntz, M., Von Bloh, W., Bounama, C., Franck, S. 2003, Icarus, 162, 215

- Danner, R., Unwin, S. 1999, SIM: Taking the Measure of the Universe, NASA/JPL
- Eisner, J. A., Kulkarni, S. R. 2001a, ApJ, 550, 871
- Eisner, J. A., Kulkarni, S. R. 2001b, ApJ, 561, 1107
- Eisner, J. A., Kulkarni, S. R. 2002, ApJ, 574, 426
- Fischer, D. A., Marcy, G. W., Butler, R. P., Vogt, S. S., Frink, S., Apps, K. 2001, ApJ, 551, 1107
- Fischer, D. A., Marcy, G. W., Butler, R. P., Laughlin, G., Vogt, S. S. 2002, ApJ, 564, 1028
- Fischer, D. A., et al. 2003, ApJ, 586, 1394
- Franz, O. G., et al. 1998, AJ, 116, 1432
- Gilliland, R. L., Baliunas, S. L. 1987, ApJ, 314, 766
- Gladman, B. 1993, Icarus, 106, 247
- Godździwski, K., Maciejewski, A. J. 2001, ApJ, 563, L81
- Godździwski, K., Bois, E., Maciejewski, A. J. 2002, MNRAS, 332, 839
- Godździwski, K. 2002, A&A, 393, 997
- Godździwski, K. 2003a, A&A, 398, 315
- Godździwski, K. 2003b, A&A, 398, 1151
- Godździwski, K., Maciejewski, A. J. 2003, ApJ, 586, L153
- Green, R. 1985, Spherical Astronomy, Cambridge University Press
- Guirado, J. C., et al. 1997, ApJ, 490, 835
- Heintz, W. D. 1978, Double Stars, Boston D. Reidel Publishing Company
- Henry, G. W., Marcy, G. W., Butler, R. P., Vogt, S. S. 2000, ApJ, 529, L41
- Horne, J. H., Baliunas, S. L. 1986, ApJ, 302, 757
- Jensen, O. G., Ulrych, T. 1973, AJ, 78, 1104
- Ji, J., Li, G., Liu, L. 2002, ApJ, 572, 1041
- Ji, J., Kinoshita, H., Liu, L., Li, G. 2003, ApJ, 585, L139
- Jiang, I., Ip, W. 2001, A&A, 367, 943
- Jones, B. W., Sleep, P. N., Chambers, J. E. 2001, A&A, 366, 254

- Jones, B. W., Sleep, P. N. 2002a, *A&A*, 393, 1015
- Jones, B. W., Sleep, P. N. 2002b, in *Scientific Frontiers in Research on Extrasolar Planets*, ed. D. Deming and S. Seager, ASP Conf. Series, 294, 225
- Jones, H. R. A., Butler, R. P., Marcy, G. W., Tinney, C. G., Penny, A. J., McCarthy, C., Carter, B. D. 2002, *MNRAS*, 337, 1170
- Kasting, J. F., Whitmire, D. P., Reynolds, R. T. 1993, *Icarus*, 101, 108
- Kells, L. M., Kern, W. F., Bland, J. R. 1942, *Spherical Trigonometry with Naval and Military Applications*, New York: McGraw-Hill
- Kinoshita, H., Nakai, H. 2001, *PASJ*, 53, L25
- Kiseleva-Eggleton, L., Bois, E., Rambaux, N., Dvorak, R. 2002, *ApJ*, 578, L145
- Konacki, M., Maciejewski, A. J., Wolszczan, A. 2002, *ApJ*, 567, 566
- Konacki, M., Torres, G., Jha, S., Sasselov, D. 2003, *Nature*, 421, 507
- Laskar, J. 1994, *A&A*, 287, L9
- Lattanzi, M. G., Spagna, A., Sozzetti, A., Casertano, S. 2000, *MNRAS*, 317, 211
- Laughlin, G., Adams, F. C. 1999, *ApJ*, 526, 881
- Laughlin, G., Chambers, J. E. 2001, *ApJ*, 551, L109
- Laughlin, G., Chambers, J. E., Fischer, D. A. 2002, *ApJ*, 579, 455
- Lee, M. H., Peale, S. J. 2002a, *ApJ*, 567, 596
- Lee, M. H., Peale, S. J. 2002b, in *Scientific Frontiers in Research on Extrasolar Planets*, ed. D. Deming and S. Seager, ASP Conf. Series, 294, 197
- Lissauer, J. J. 1993, *ARA&A*, 31, 129
- Marcy, G. W., Benitz, K. J. 1989, *ApJ*, 344, 441
- Marcy G. W., Butler R. P., Fischer D., et al. 2001a, *ApJ*, 556, 296
- Marcy G. W., Butler R. P., Vogt S. S., et al. 2001b, *ApJ*, 555, 418
- Marcy, G. W., Butler, R. P., Fischer, D. A., Vogt, S. S. 2002a, in *Scientific Frontiers in Research on Extrasolar Planets*, ed. D. Deming and S. Seager, ASP Conf. Series, 294, 1
- Marcy, G. W., Butler, R. P., Fischer, D. A., Laughlin, G., Vogt, S. S., Henry, G. W., Pourbaix, D. 2002b, *ApJ*, 581, 1375

- Mariotti, J. M., et al. 1998, Proc. SPIE 3350, Astronomical Interferometry, Ed. R. D. Reasenberg, p. 800
- Mayer, L., Quinn, T., Wadsley, J., Stadel, J. 2002, Science, 298, 1756
- Mayor, M., et al. 2001, ESO Press Release 07/01
- Mazeh, T., et al. 2000, ApJ, 532, L55
- Menou, C., Tabachnik, S. 2003, ApJ, 583, 473
- Monet, D. G. 1983, in Current Techniques in Double and Multiple Star Research, ed. R. S. Harrington and O. G. Franz, IAU Coll., 62, 286
- Nagasawa, M., Lin, D. N. C., Ida, S. 2003, ApJ, 586, 1374
- Nelson, A. F., Angel, J. R. P. 1998, ApJ, 500, 940
- Nelson, R. P., Papaloizou, J. C. B. 2002, MNRAS, 333, L26
- Noble, M., Musielak, Z. E., Cuntz, M. 2002, ApJ, 572, 1024
- Novak, G. S., Lai, D., Lin, D. N. C. 2002, in Scientific Frontiers in Research on Extrasolar Planets, ed. D. Deming and S. Seager, ASP Conf. Series, 294, 177
- Perryman, M. A. C., et al. 2001, A&A, 369, 339
- Pollack, J. B., Hubickyj, O., Bodenheimer, P., Lissauer, J. J., Podolack, M., Greenzweig, Y. 1996, Icarus, 124, 62
- Pourbaix, D., Jorissen, A. 2000, A&AS, 145, 161
- Press, W. H., Rybicki, G. B. 1989, ApJ, 338, 277
- Press, W. H., Teukolsky, S. A., Vetterling, V. T., Flannery, B. P. 1992, Numerical Recipes in FORTRAN: the Art of Scientific Computing, Cambridge University Press
- Queloz, D., et al. 2000, A&A, 359, L13
- Rivera, E. J., Lissauer, J. J. 2000, ApJ, 530, 454
- Rivera, E. J., Lissauer, J. J. 2001a, ApJ, 554, 1141
- Rivera, E. J., Lissauer, J. J. 2001b, ApJ, 558, 392
- Rivera, E. J., Haghighipour N. 2002, in Scientific Frontiers in Research on Extrasolar Planets, ed. D. Deming and S. Seager, ASP Conf. Series, 294, 205
- Scargle, J. D. 1982, ApJ, 263, 835

- Schwarzenberg-Czerny, A. 1996, ApJ, 460, L107
- Snellgrove, M. D., Papaloizou, J. C. B., Nelson, R. P. 2001, A&A, 374, 1092
- Sozzetti, A., Casertano, S., Lattanzi, M. G., Spagna A. 2001, A&A, 373, L21
- Sozzetti, A., Casertano, S., Brown, R. A., Lattanzi, M. G. 2002, PASP, 114, 1173 (S02)
- Stepinski, T. F., Malhotra, R., Black, D.C. 2000, ApJ, 545, 1044
- Sussman, G. J., Wisdom, J. 1992, Science, 257, 56
- Thébaud, P., Marzari, F., Scholl, H. 2002, A&A, 384, 594
- Udry, S., Mayor, M., Naef, D., Pepe, F., Queloz, D., Santos, N. C., Burnet, M. 2002, A&A, 390, 267
- Walker, G. A. H., Walker, A. R., Irwin, A. W., Larson, A. M., Yang, S. L. S., Richardson, D. C. 1995, Icarus, 116, 359
- Wolszczan, A., Frail, D. A. 1992, Nature, 355, 145

Fig. 1.— Probability of detection as a function of orbital inclination i , for each planet in each of the 11 multiple-planet systems considered in our study. The three planets HD 38529 b (dashed-dotted-dotted line), ν And b (long-dashed line), and 55 Cnc c (dashed-dotted line) are the most difficult to detect. After the not accurate subtraction of their low-amplitude astrometric signatures, the corresponding false detection rates are up to a factor 2 larger than the expected 5%

Fig. 2.— Periodogram analysis for the HD 38529 planetary system. In the upper left panel we show the periodicity search after the single-star fit: a long-period signal is clearly found with high significance, but due to the incomplete orbital sampling, its value is about a factor 2 shorter than the actual period of HD 38529 c. The upper right panel highlights how, after the removal of the signal with the larger amplitude, the period of HD 38529 b is still accurately identified, in spite of the very low astrometric signature induced by the inner planet of the system on its central star. The lower left panel presents the results of the periodogram analysis after the dual Keplerian fit to the observations: no significant peaks are found

Fig. 3.— Same as Figure 2, but for the ν And planetary system. The periodogram analysis correctly identifies the periods of the two outer planets (two upper panels), and rules out the presence of additional planets after subtraction of all planetary signatures (lower right panel). Due to the very short period of the innermost planet, instead, after removal of the signatures of ν And c and ν And d the periodogram search identifies a significant peak in the spectrum which does not correspond to the true period of ν And b (lower left panel)

Fig. 4.— Same as Figure 2, but for the ‘easy’ case of the HD 82943 planetary system

Fig. 5.— Same as Figure 2, but for the case of the 55 Cnc planetary system. The planet inducing the larger signature, 55 Cnc d, is identified immediately in the power spectrum (upper left panel), but, similarly to the case of HD 38529 c shown in Figure 2, the incomplete orbital sampling causes the periodogram analysis to identify an incorrect value for the orbital period of 55 Cnc d

Fig. 6.— Reduced chi-square χ^2_{ν} as a function of a dense grid of trial periods for the five planetary systems harboring one planet with a period exceeding the timespan of SIM observations (two upper, two middle, and lower left panels). For comparison, the lower right panel shows the results of the same procedure applied to our own solar system, placed at increasing distance from the observer (details in the text)

Fig. 7.— Fractional errors (%) for M_p , a , T , e , and i , as a function of the inclination of the orbital plane, in the case of the 55 Cnc planetary system. In each panel, the results for a given parameter are shown for all the system components, for the cases of a single-planet solution (dashed-dotted, dotted, and short-dashed lines for 55 Cnc b, 55 Cnc c, and 55 Cnc d, respectively) and a complete three-planet model (solid, long-dashed, and dashed-dotted-dotted lines for 55 Cnc b, 55 Cnc c, and 55 Cnc d, respectively)

Fig. 8.— Same as Figure 7, but for the case of the HD 12661 planetary system. The dashed-dotted and dashed-dotted-dotted lines are relative to the single-planet solution for HD 12661 b and HD 12661 c, respectively. The solid and long-dashed lines are relative to the dual Keplerian fit for HD 12661 b and HD 12661 c, respectively

Fig. 9.— Iso-accuracy contours in the $e - T$ plane, for the most relevant orbital parameters and planet mass. The results in each panel have been obtained utilizing the 11 planetary systems known to-date. The contour regions are color-coded by the accuracy achieved in the determination of the given parameter, expressed as a fraction (%) of its true value

Fig. 10.— Same as Figure 9, but with the contour regions identified in the $\alpha/\sigma_d - T$ plane

Fig. 11.— Relative inclination i_{rel} between pairs of planetary orbits as a function of the common inclination angle with respect to the line of sight, for the entire set of presently known multiple-planet systems. In each panel, the corresponding uncertainties are computed utilizing the formal expressions from the covariance matrix of the multiple Keplerian fit

Fig. 12.— Contours identifying regions, in the $\alpha/\sigma_d - T$ plane, with equal values of the ratios σ_G/σ_C of the estimated fractional uncertainties on M_p , a , and i in the case of ‘global’ fits in which all parameters were adjusted to the same quantities as computed after the ‘constrained’ fits (as discussed in the text), for the set of presently known planetary systems. The results are averaged over the inclination angle (coplanar orbits are assumed). The contour regions are color-coded by the value of the ratio σ_G/σ_C for each parameter

Fig. 13.— The behavior of the ratios σ_G/σ_C for M_p (upper panels), a (middle panels), and i (lower panels), expressed as a function of the common inclination angle, for the two representative multiple-planet systems 55 Cnc and 47 UMa

Fig. 14.— Same as Figure 13, but for the HD 12661 and HD 38529 planetary systems

Table 1. Fundamental stellar characteristics, astrometric parameters and orbital elements of the presently known set of extra-solar planetary systems utilized in the simulations. Planet masses and astrometric signatures are computed as lower limits corresponding to edge-on configurations ($\sin i = 1$). The data have been taken utilizing various web resources containing up-to-date values of all parameters, as explained in the notes

Stellar Parameters ^a	Central Star	Orbital elements ^b	Planet b	Planet c	Planet d
System: <i>v</i> And					
λ (deg)	38.36	α (μas)	2.32	89.58	541.8
β (deg)	29.25	a (AU)	0.059	0.83	2.53
μ_λ (mas/yr)	−313.16	T (d)	4.6	241.5	1284.0
μ_β (mas/yr)	−277.30	e	0.012	0.28	0.27
π (mas)	74.25	τ (JD)	2450002.1	2450160.5	2450064.0
V Magnitude	4.09	ω (deg)	73.0	250.0	260.0
Spectral Type	F8V	$M_p \sin i$ (M_J)	0.69	1.89	3.75
d (pc)	13.47	Ω (deg)	$[0, \pi]$	$[0, \pi]$	$[0, \pi]$
M_\star (M_\odot)	1.3	i (deg)	$[0, \pi/2]$	$[0, \pi/2]$	$[0, \pi/2]$
System: 55 Cnc					
λ (deg)	127.79	α (μas)	7.75	4.04	1916.6
β (deg)	10.70	a (AU)	0.115	0.24	5.9
μ_λ (mas/yr)	−530.91	T (d)	14.653	44.28	5360.0
μ_β (mas/yr)	−93.54	e	0.02	0.34	0.16
π (mas)	79.81	τ (JD)	2450001.479	2450031.4	2452785.0
V Magnitude	5.95	ω (deg)	99.0	61.0	201.0
Spectral Type	G8V	$M_p \sin i$ (M_J)	0.84	0.21	4.05
d (pc)	12.53	Ω (deg)	$[0, \pi]$	$[0, \pi]$	$[0, \pi]$
M_\star (M_\odot)	0.95	i (deg)	$[0, \pi/2]$	$[0, \pi/2]$	$[0, \pi/2]$
System: HD 38529					
λ (deg)	86.23	α (μas)	1.71	805.7	...
β (deg)	−21.78	a (AU)	0.129	3.71	...
μ_λ (mas/yr)	−83.66	T (d)	14.31	2207.4	...
μ_β (mas/yr)	−139.69	e	0.28	0.33	...

Table 1—Continued

Stellar Parameters ^a	Central Star	Orbital elements ^b	Planet b	Planet c	Planet d
π (mas)	23.58	τ (JD)	24510005.8	24510043.7	...
V Magnitude	5.95	ω (deg)	90.0	13.0	...
Spectral Type	G4IV	$M_p \sin i$ (M_J)	0.78	12.8	...
d (pc)	42.40	Ω (deg)	$[0, \pi]$	$[0, \pi]$...
M_\star (M_\odot)	1.39	i (deg)	$[0, \pi/2]$	$[0, \pi/2]$...
System: Gliese 876					
λ (deg)	339.21	α (μas)	264.4	48.5	...
β (deg)	−6.77	a (AU)	0.21	0.13	...
μ_λ (mas/yr)	634.86	T (d)	61.02	30.12	...
μ_β (mas/yr)	−987.72	e	0.10	0.27	...
π (mas)	213.22	τ (JD)	2450106.2	2450031.4	...
V Magnitude	10.15	ω (deg)	333.0	330.0	...
Spectral Type	M4	$M_p \sin i$ (M_J)	1.89	0.56	...
d (pc)	4.69	Ω (deg)	$[0, \pi]$	$[0, \pi]$...
M_\star (M_\odot)	0.32	i (deg)	$[0, \pi/2]$	$[0, \pi/2]$...
System: HD 168443					
λ (deg)	225.07	α (μas)	58.64	1269.5	...
β (deg)	13.33	a (AU)	0.295	2.87	...
μ_λ (mas/yr)	−99.95	T (d)	58.10	1771.5	...
μ_β (mas/yr)	−220.79	e	0.53	0.20	...
π (mas)	25.97	τ (JD)	2450047.6	2450250.0	...
V Magnitude	6.91	ω (deg)	172.9	289.0	...
Spectral Type	G5IV	$M_p \sin i$ (M_J)	7.73	17.2	...
d (pc)	38.5	Ω (deg)	$[0, \pi]$	$[0, \pi]$...
M_\star (M_\odot)	1.01	i (deg)	$[0, \pi/2]$	$[0, \pi/2]$...

Table 1—Continued

Stellar Parameters ^a	Central Star	Orbital elements ^b	Planet b	Planet c	Planet d
System: HD 12661					
λ (deg)	37.70	α (μas)	47.43	100.4	...
β (deg)	12.26	a (AU)	0.82	2.56	...
μ_λ (mas/yr)	−161.28	T (d)	263.3	1444.5	...
μ_β (mas/yr)	−127.78	e	0.35	0.20	...
π (mas)	26.91	τ (JD)	2459943.7	2459673.9	...
V Magnitude	7.43	ω (deg)	292.6	147.0	...
Spectral Type	G6V	$M_p \sin i$ (M_J)	2.30	1.56	...
d (pc)	37.16	Ω (deg)	$[0, \pi]$	$[0, \pi]$...
M_\star (M_\odot)	1.07	i (deg)	$[0, \pi/2]$	$[0, \pi/2]$...
System: HD 160691 ^c					
λ (deg)	267.20	α (μas)	155.8	139.2	...
β (deg)	−28.87	a (AU)	1.48	2.30	...
μ_λ (mas/yr)	−20.96	T (d)	637.3	1300.0	...
μ_β (mas/yr)	−190.61	e	0.31	0.8	...
π (mas)	65.36	τ (JD)	2450959.0	2451613.0	...
V Magnitude	5.15	ω (deg)	320.0	99.0	...
Spectral Type	G3IV/V	$M_p \sin i$ (M_J)	1.74	1.0	...
d (pc)	15.30	Ω (deg)	$[0, \pi]$	$[0, \pi]$...
M_\star (M_\odot)	1.08	i (deg)	$[0, \pi/2]$	$[0, \pi/2]$...
System: 47 UMa					
λ (deg)	149.30	α (μas)	366.1	195.5	...
β (deg)	31.28	a (AU)	2.09	3.73	...
μ_λ (mas/yr)	−259.16	T (d)	1089.0	2594.0	...
μ_β (mas/yr)	188.90	e	0.06	0.10	...
π (mas)	71.02	τ (JD)	2453622.0	2451363.5	...

Table 1—Continued

Stellar Parameters ^a	Central Star	Orbital elements ^b	Planet b	Planet c	Planet d
V Magnitude	5.03	ω (deg)	172.0	127.0	...
Spectral Type	G0V	$M_p \sin i$ (M_J)	2.54	0.76	...
d (pc)	14.08	Ω (deg)	[0, π]	[0, π]	...
M_\star (M_\odot)	1.03	i (deg)	[0, $\pi/2$]	[0, $\pi/2$]	...
System: HD 82943 ^d					
λ (deg)	150.22	α (μas)	65.58	22.28	...
β (deg)	−24.79	a (AU)	1.16	0.73	...
μ_λ (mas/yr)	−58.14	T (d)	444.6	221.6	...
μ_β (mas/yr)	−164.07	e	0.41	0.54	...
π (mas)	36.42	τ (JD)	2451620.3	2451630.9	...
V Magnitude	6.54	ω (deg)	96.0	138.0	...
Spectral Type	G0	$M_p \sin i$ (M_J)	1.63	0.88	...
d (pc)	27.46	Ω (deg)	[0, π]	[0, π]	...
M_\star (M_\odot)	1.05	i (deg)	[0, $\pi/2$]	[0, $\pi/2$]	...
System: HD 74156 ^d					
λ (deg)	131.71	α (μas)	6.35	383.9	...
β (deg)	−12.86	a (AU)	0.276	3.47	...
μ_λ (mas/yr)	−28.19	T (d)	51.61	2300.0	...
μ_β (mas/yr)	−200.05	e	0.65	0.40	...
π (mas)	15.49	τ (JD)	2451981.4	2450849.0	...
V Magnitude	7.62	ω (deg)	183.7	240.0	...
Spectral Type	G0	$M_p \sin i$ (M_J)	1.56	7.5	...
d (pc)	64.56	Ω (deg)	[0, π]	[0, π]	...
M_\star (M_\odot)	1.05	i (deg)	[0, $\pi/2$]	[0, $\pi/2$]	...

Table 1—Continued

Stellar Parameters ^a	Central Star	Orbital elements ^b	Planet b	Planet c	Planet d
System: HD 37124					
λ (deg)	84.62	α (μas)	15.37	98.62	...
β (deg)	−2.17	a (AU)	0.54	2.95	...
μ_λ (mas/yr)	−96.14	T (d)	153.0	1942.0	...
μ_β (mas/yr)	−416.51	e	0.10	0.40	...
π (mas)	30.12	τ (JD)	2451227.0	2451828.0	...
V Magnitude	7.68	ω (deg)	97.0	265.0	...
Spectral Type	G4V	$M_p \sin i$ (M_J)	0.86	1.01	...
d (pc)	33.20	Ω (deg)	$[0, \pi]$	$[0, \pi]$...
M_\star (M_\odot)	0.91	i (deg)	$[0, \pi/2]$	$[0, \pi/2]$...

^aData from <http://simbad.u-strasbg.fr/>. Positions and proper motion components, originally given in equatorial coordinates, have been projected to the ecliptic reference frame (see for example Green 1985)

^bData from <http://www.obspm.fr/encycl/encycl.html> and <http://exoplanets.org/> as of September 2002

^cThe existence of the outer planet around HD 160691 is still doubtful. Its presence has been inferred by Jones et al. (2002), due to a clear trend in the radial velocity residuals, but the orbit still awaits phase closure

^dThe discovery of the planetary systems around HD 74156 and HD 82943 has not yet been reported in refereed Journals

Table 2. Results from the periodogram analysis of the 11 planetary systems known to date, in the case of an average value of the orbital inclination angle ($i = 45^\circ$). The columns display, respectively, the name of the system, the type of fit performed (single-star, single- or multiple-planet), the value of the reduced chi-square χ_ν^2 of the fit, the highest peak z_p in the periodogram power spectrum, the value of the orbital period $T(z_p)$ corresponding to the peak in the spectrum, and the false-alarm probability $P(z_p)$ of the peak

System	Type of Fit	χ_ν^2	z_p	$T(z_p)$	$P(z_p)$
<i>v</i> And	Single Star	3096.55	50.6828	3.75855	0.0
	1 Planet	1736.20	48.5907	0.671169	0.0
	2 Planets	1.87563	14.6750	0.119567	6.35×10^{-5}
	3 Planets	1.14677	8.41723	0.220069	0.0326138
55 Cnc	Single Star	1856.12	65.3129	5.87275	0.0
	1 Planet	25.3619	51.3840	0.0401112	0.0
	2 Planets	4.13032	39.1092	0.121448	0.0
	3 Planets	0.791748	4.85446	0.0705180	0.690751
HD 38529	Single Star	1063.33	35.7711	3.49768	0.0
	1 Planet	1.46852	28.3746	0.0389847	1.37×10^{-9}
	2 Planets	0.974422	6.45905	0.0402565	0.209530
Gliese 876	Single Star	583.995	57.6141	0.166749	0.0
	1 Planet	392.007	53.6403	0.0821299	0.0
	2 Planets	0.720508	7.41911	0.393050	0.0860501
HD 168443	Single Star	13919.0	54.8187	4.50731	0.0
	1 Planet	534.999	42.8020	0.157193	0.0
	2 Planets	0.943551	6.85225	0.109261	0.146701
HD 12661	Single Star	67.2261	28.1816	3.30105	1.23×10^{-7}
	1 Planet	481.436	44.0427	0.741820	0.0
	2 Planets	1.13029	6.83758	0.0402566	0.148699
HD 160691	Single Star	225.807	50.5789	1.65052	0.0
	1 Planet	1650.87	56.9019	3.27908	0.0
	2 Planets	0.857078	7.96351	0.397465	0.0508595
47 UMa	Single Star	688.689	42.7118	2.81892	0.0
	1 Planet	402.954	51.3840	4.95227	1.35×10^{-9}
	2 Planets	1.04254	4.81968	0.1009260	0.703383

Table 2—Continued

System	Type of Fit	χ^2_ν	z_p	$T(z_p)$	$P(z_p)$
HD 82943	Single Star	29.2090	53.8883	1.23789	0.0
	1 Planet	36.8078	43.9404	0.618946	0.0
	2 Planets	1.01055	5.77669	0.0398152	0.372220
HD 74156	Single Star	224.126	48.2071	3.30105	0.0
	1 Planet	4.25179	36.1520	0.140470	0.0
	2 Planets	0.994640	5.25626	0.0330859	0.543543
HD 37124	Single Star	82.4841	57.8993	4.36463	0.0
	1 Planet	36.8113	39.9654	0.415679	0.0
	2 Planets	0.931258	5.95232	0.0394809	0.321418

Table 3. Ranges of plausible starting guesses for the orbital period of the 5 planets with $T > 5$ yr in the presently known extrasolar multiple-planet systems. For reference, the same results are reported for Jupiter in simulations of the solar system as ‘seen’ by SIM at increasing distances (in pc) from the observer. The results are derived in the context of the Fourier analysis approach discussed in the text. Preliminary values of T are considered acceptable if the corresponding χ_ν^2 does not differ from the minimum $\chi_{\nu,\min}^2$ by more than $\pm 15\%$ of the latter value

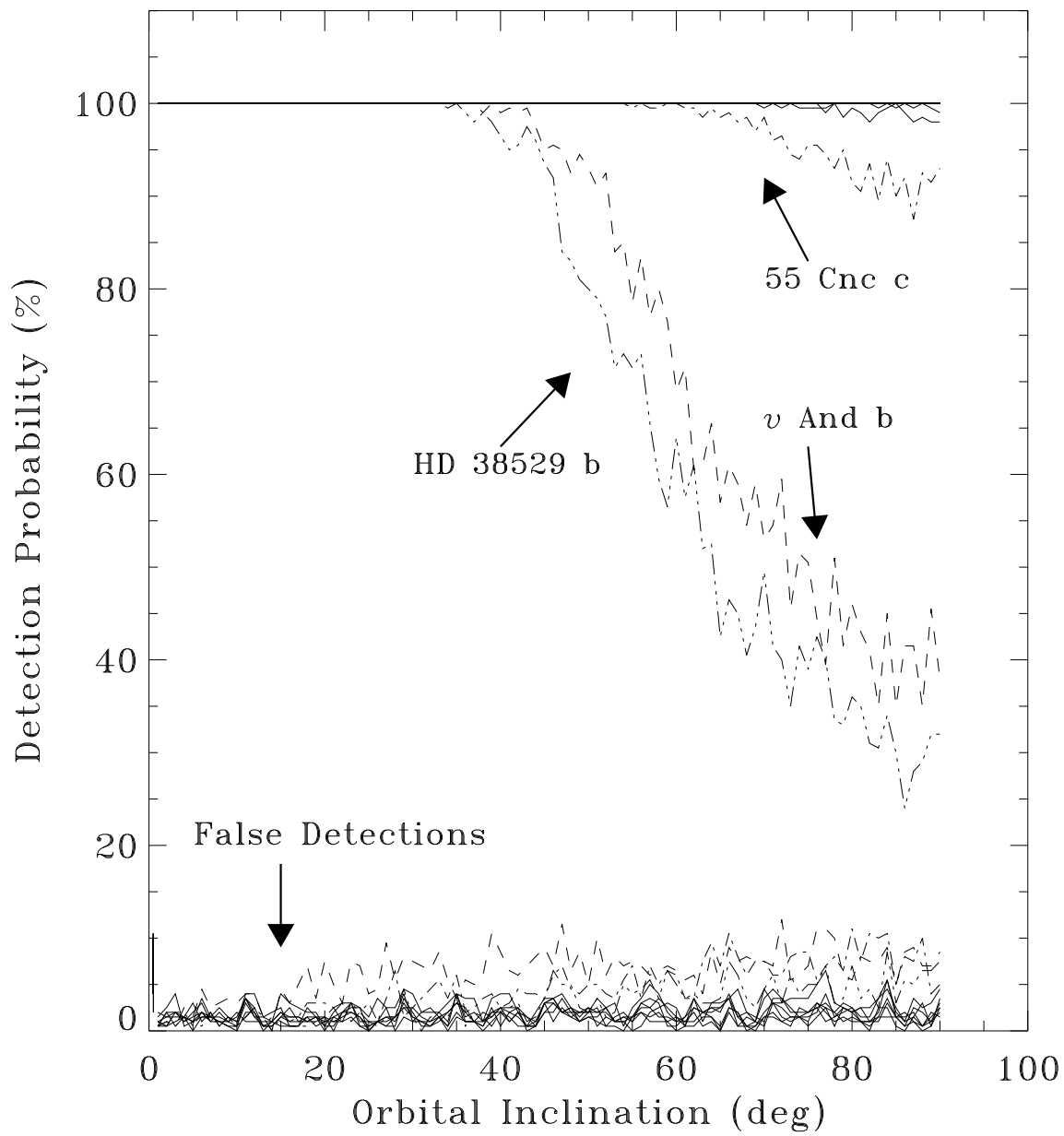
Planet	Plausible χ_ν^2 Ranges	Plausible T Ranges
HD 37124 c	$28.62 \leq \chi_\nu^2 \leq 38.72$	$4.69 \leq T \leq 7.12$ yr
HD 74156 c	$5.40 \leq \chi_\nu^2 \leq 7.31$	$5.85 \leq T \leq 6.38$ yr
HD 38529 c	$1.17 \leq \chi_\nu^2 \leq 0.86$	$5.93 \leq T \leq 6.08$ yr
55 Cnc d	$19.46 \leq \chi_\nu^2 \leq 26.33$	$12.99 \leq T \leq 16.25$ yr
47 UMa c	$0.66 \leq \chi_\nu^2 \leq 0.90$	$5.91 \leq T \leq 9.22$ yr
Jupiter (2 pc)	$1.07 \leq \chi_\nu^2 \leq 1.45$	$11.11 \leq T \leq 11.61$ yr
Jupiter (3 pc)	$0.87 \leq \chi_\nu^2 \leq 1.18$	$10.98 \leq T \leq 11.66$ yr
Jupiter (10 pc)	$0.70 \leq \chi_\nu^2 \leq 0.95$	$10.16 \leq T \leq 12.07$ yr

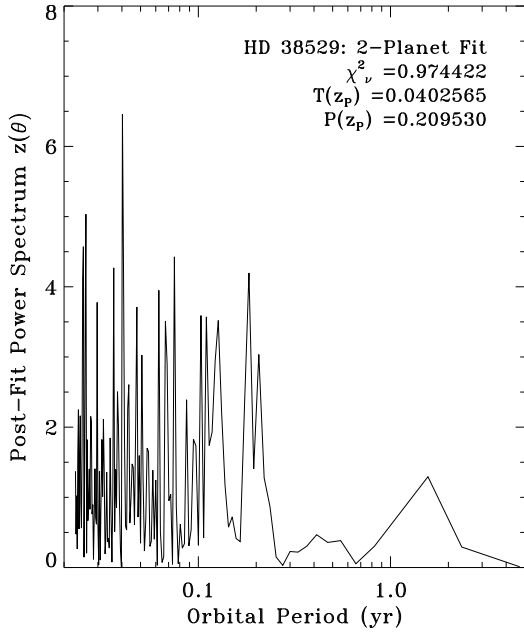
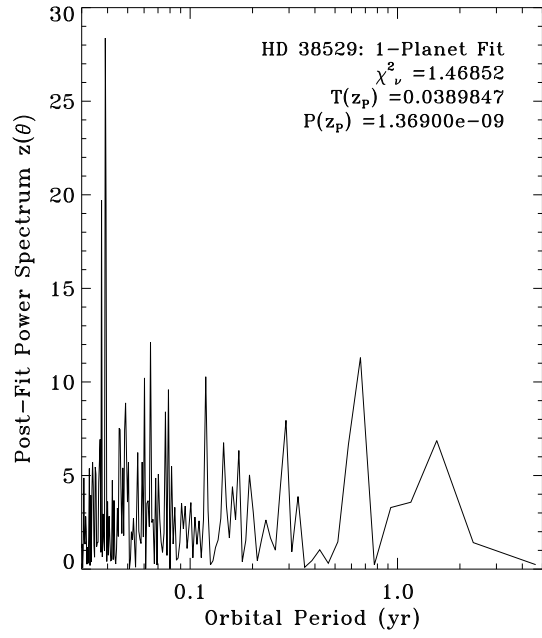
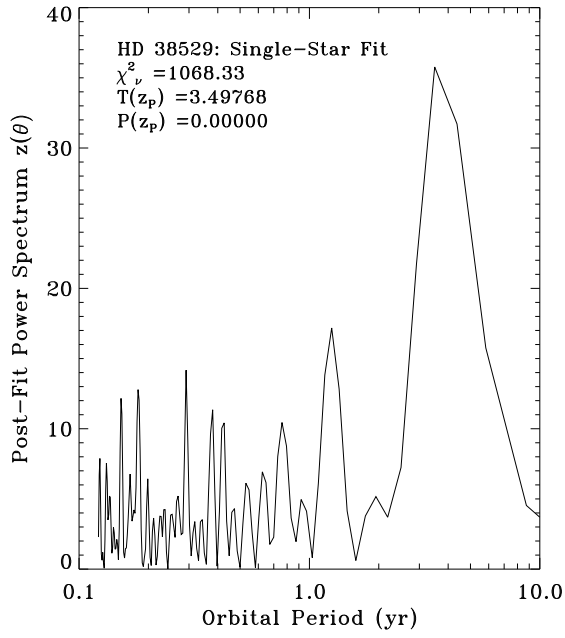
Table 4. Ratios of the rms errors σ_m for a given parameter (M_p , a , T , e , and i) derived from a multiple-planet fit (in simulations where the full planetary system was generated around the parent star) to the rms errors σ_s derived from a single-planet solution (in simulations where only one planet orbited the central star). The values are averaged over the inclination angle

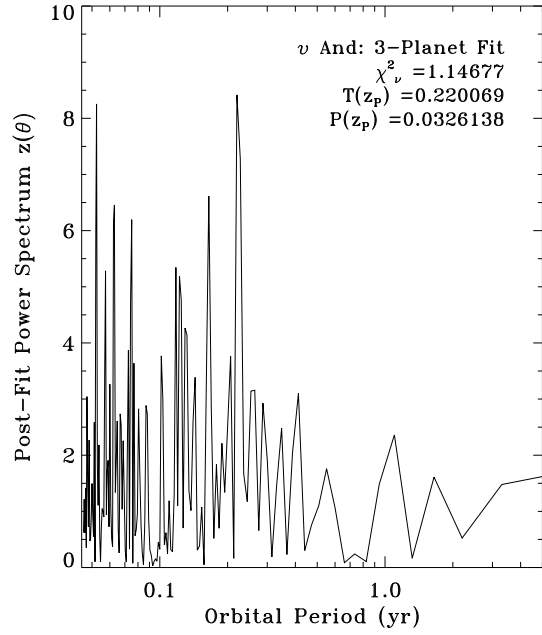
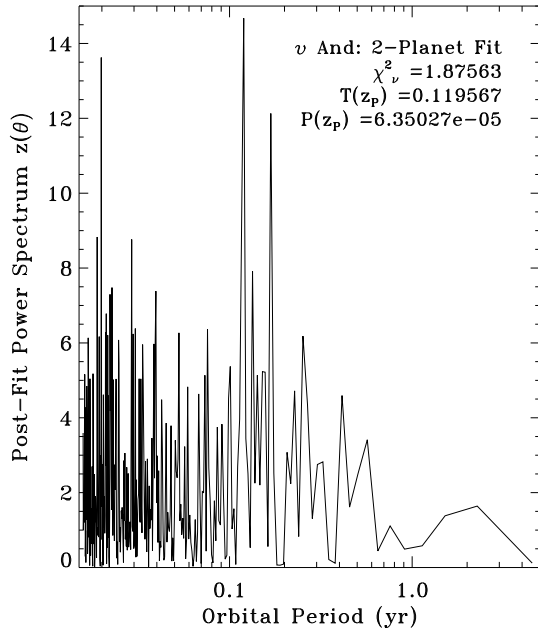
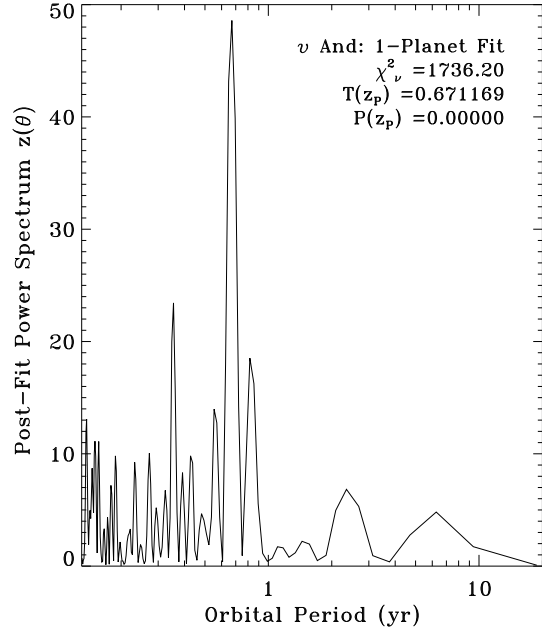
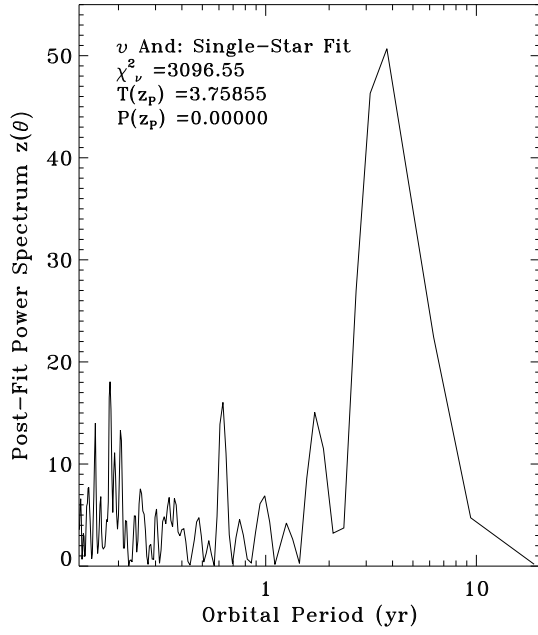
Planet	$\sigma_m(M_p)/\sigma_s(M_p)$	$\sigma_m(a)/\sigma_s(a)$	$\sigma_m(T)/\sigma_s(T)$	$\sigma_m(e)/\sigma_s(e)$	$\sigma_m(i)/\sigma_s(i)$
<i>v</i> And b	2.42	2.32	1.56	0.98	1.36
<i>v</i> And c	1.42	1.35	1.59	1.40	1.35
<i>v</i> And d	1.35	1.37	1.54	1.52	1.35
55 Cnc b	1.39	1.39	1.49	1.35	1.23
55 Cnc c	1.48	1.48	1.40	1.14	1.18
55 Cnc d	1.00	0.76	0.83	1.53	1.71
47 UMa b	15.4	18.0	9.64	1.54	2.31
47 UMa c	1.04	1.09	1.12	3.69	2.71
Gliese 876 b	1.21	1.21	1.21	1.39	1.12
Gliese 876 c	1.22	1.23	1.55	1.14	1.12
HD 12661 b	1.15	1.15	1.24	1.15	1.12
HD 12661 c	1.19	1.21	1.37	1.33	1.10
HD 160691 b	1.54	1.54	1.86	1.38	1.32
HD 160691 c	2.09	2.07	2.00	1.78	1.66
HD 168443 b	1.13	1.15	1.21	1.13	1.09
HD 168443 c	0.46	0.47	0.86	0.97	1.09
HD 37124 b	1.18	1.17	1.27	1.16	1.11
HD 37124 c	0.28	0.48	1.00	0.84	0.86
HD 38529 b	1.19	1.19	1.19	1.04	1.07
HD 38529 c	0.86	0.85	0.78	0.55	0.87
HD 74156 b	1.08	1.08	1.29	1.06	1.06
HD 74156 c	0.59	0.71	0.94	0.68	0.66
HD 82943 b	2.87	2.08	1.69	3.23	1.77
HD 82943 c	2.50	1.81	1.95	2.05	1.70

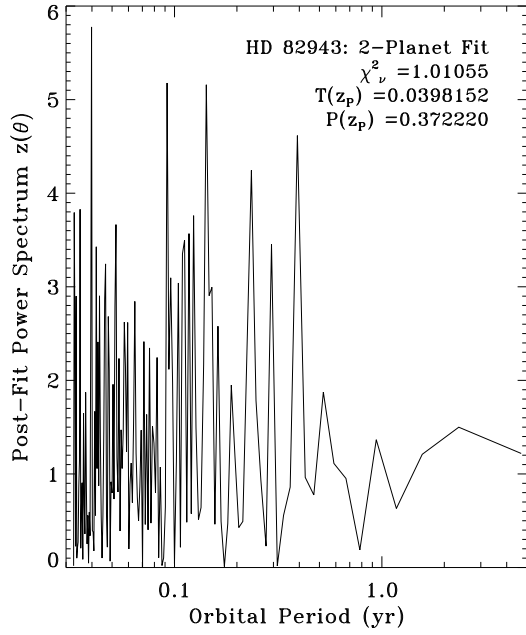
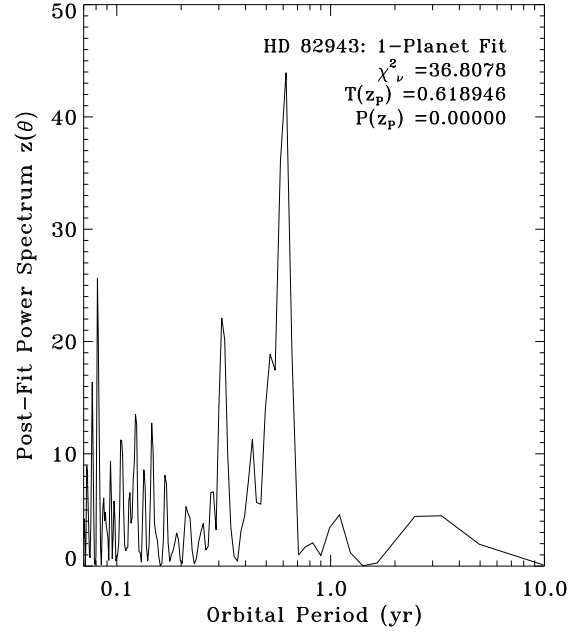
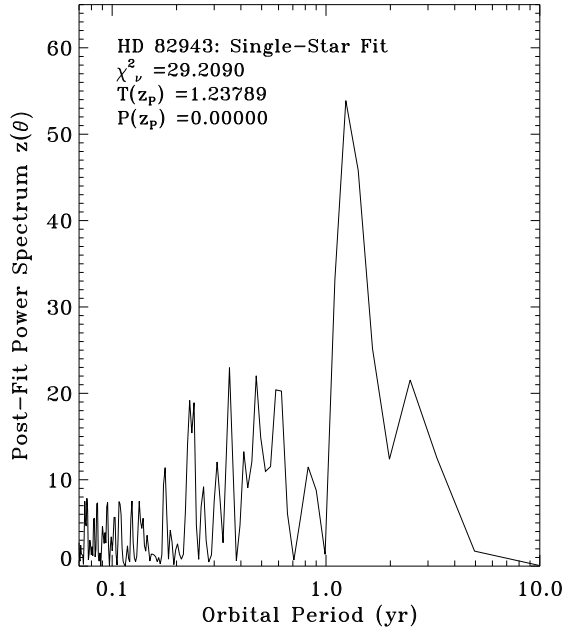
Table 5. Results from a fit to the fractional errors on orbital elements and planet mass, assuming a three-dimensional power-law dependence on the three parameters α/σ_d , T , and e of the form: $\eta_0 \times (\alpha/\sigma_d)^{\eta_1} \times T^{\eta_2} \times e^{\eta_3}$. The results are averaged over the inclination angle

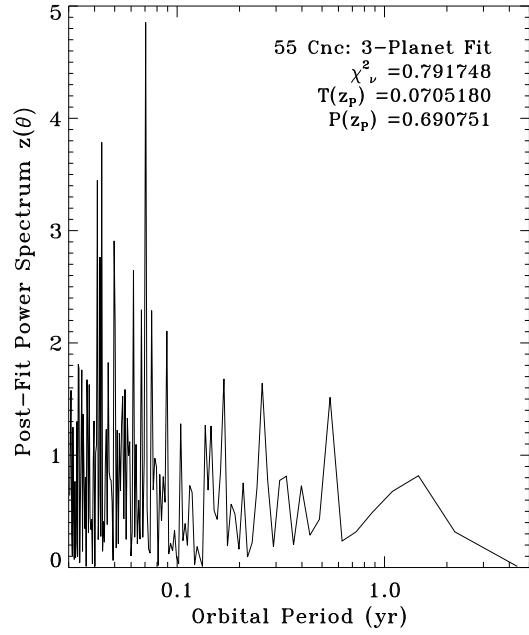
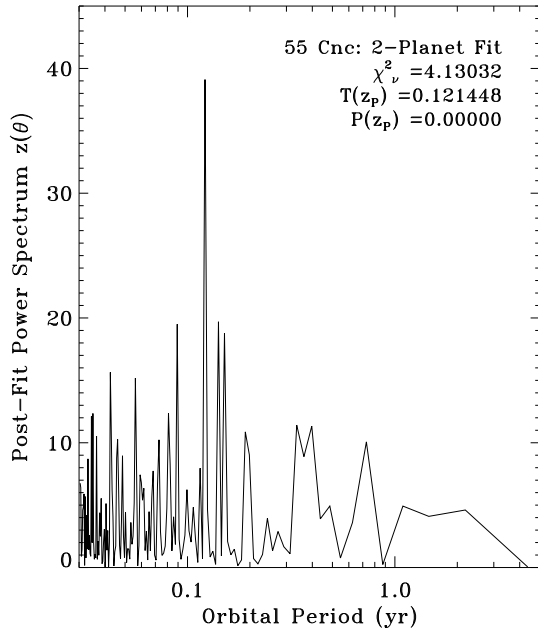
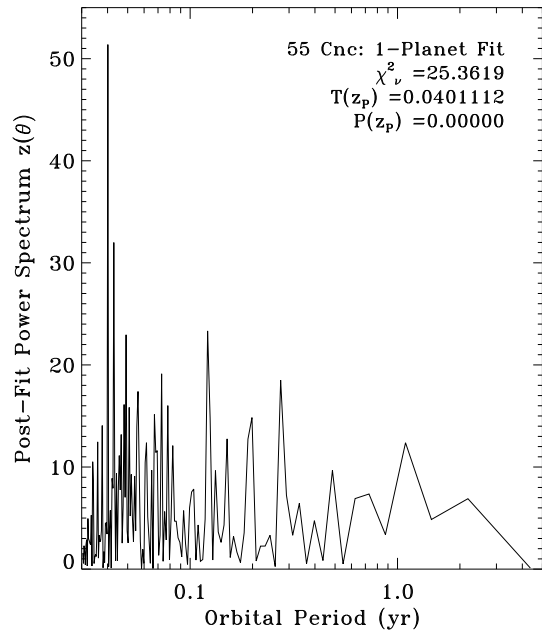
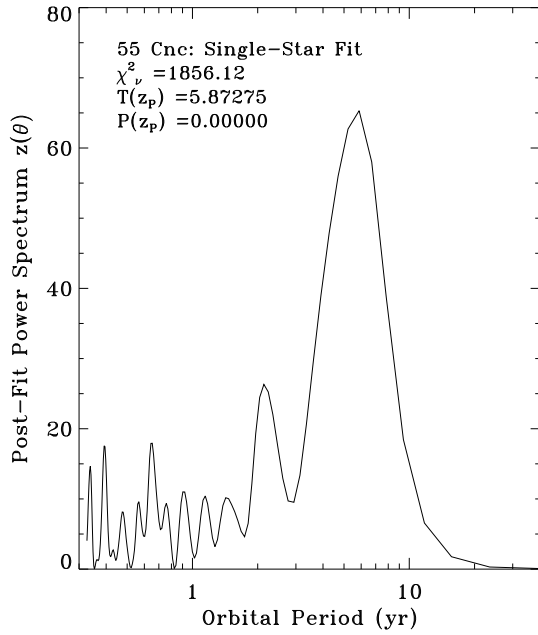
Parameter Error (%)	Best-Fit Power-Law
σ_{M_p}	$34.96 \times (\alpha/\sigma_d)^{-0.72} \times T^{-0.42} \times e^{0.35}$
σ_a	$34.08 \times (\alpha/\sigma_d)^{-0.73} \times T^{-0.43} \times e^{0.36}$
σ_T	$2.50 \times (\alpha/\sigma_d)^{-1.19} \times T^{2.65} \times e^{-0.12}$
σ_e	$23.39 \times (\alpha/\sigma_d)^{-0.87} \times T^{0.01} \times e^{-1.06}$
σ_i	$24.28 \times (\alpha/\sigma_d)^{-0.59} \times T^{-0.13} \times e^{0.08}$
σ_Ω	$67.85 \times (\alpha/\sigma_d)^{-0.43} \times T^{-0.06} \times e^{0.43}$

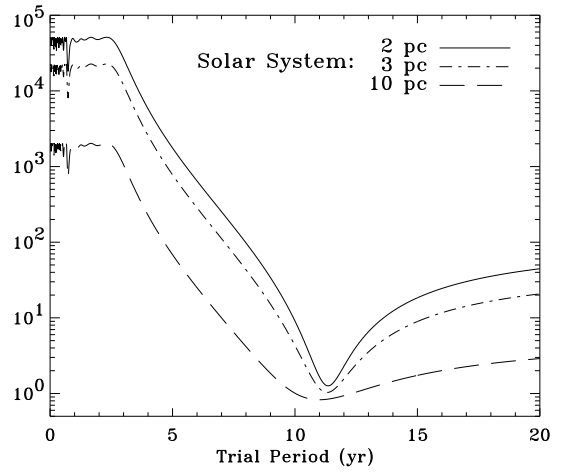
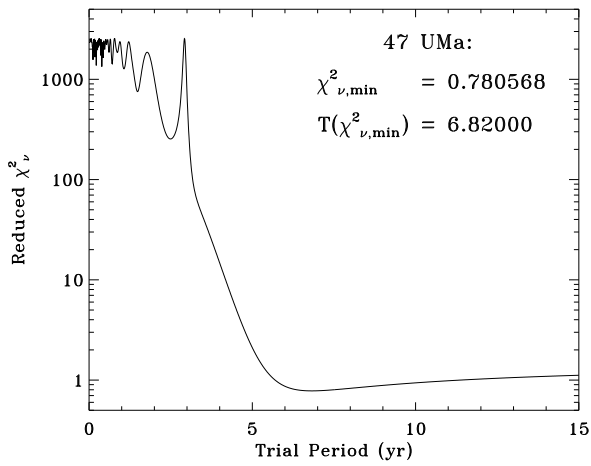
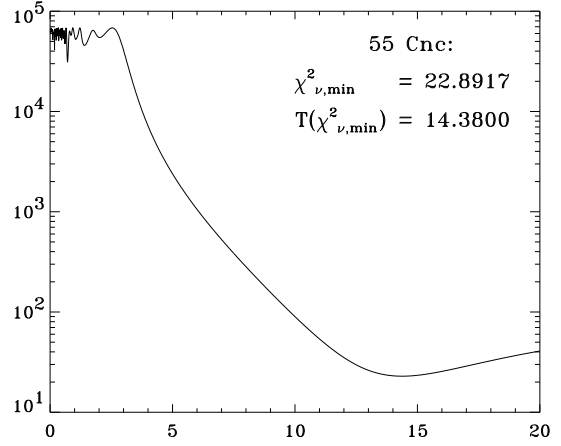
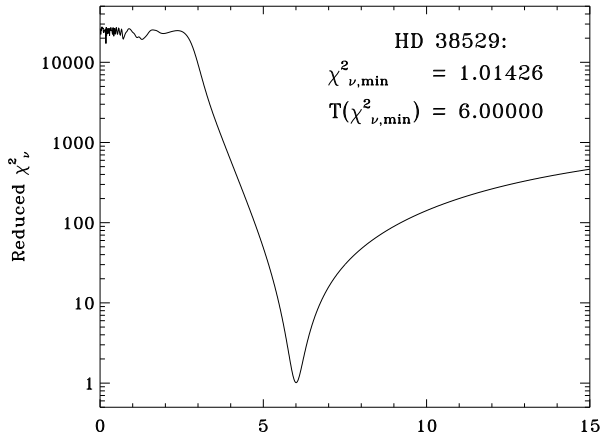
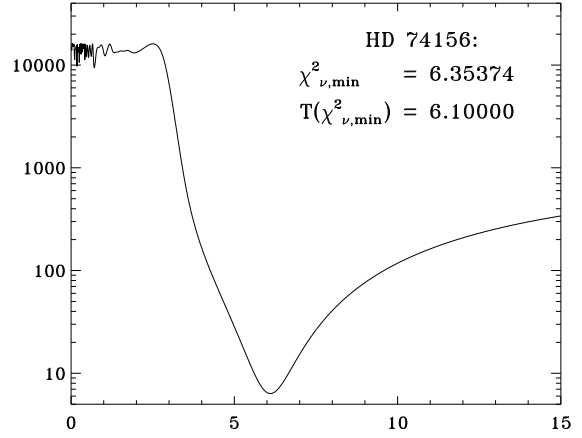
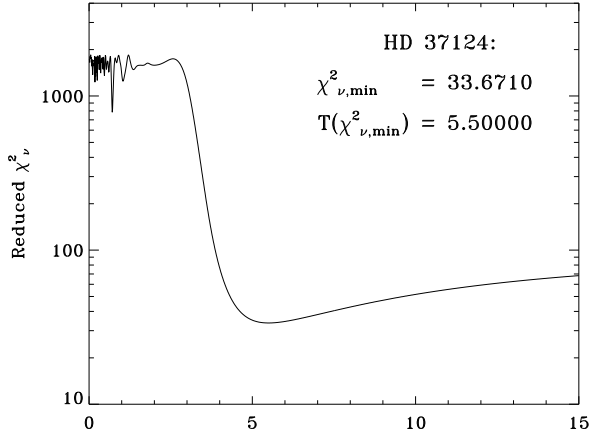


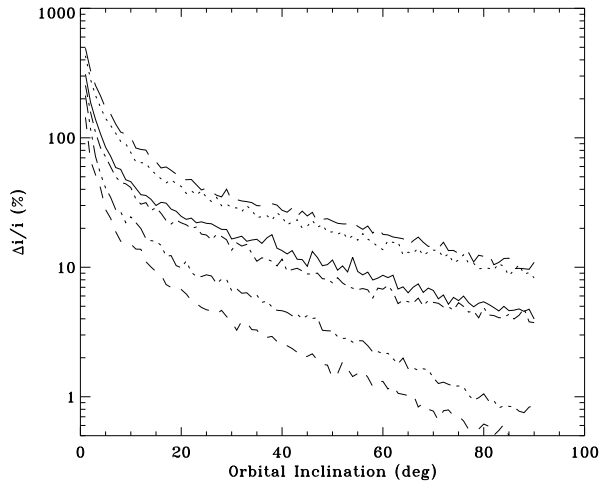
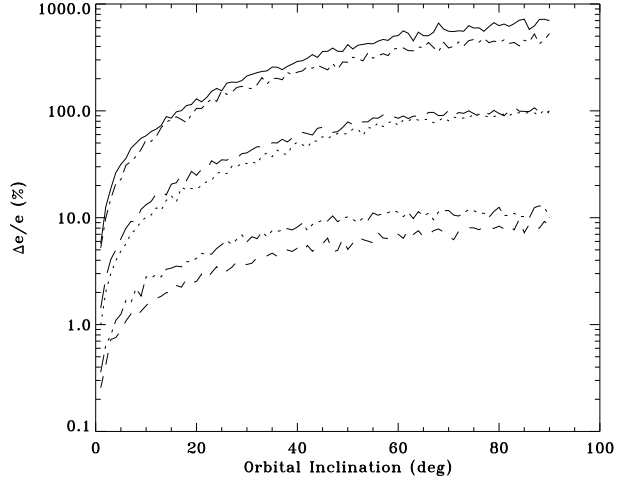
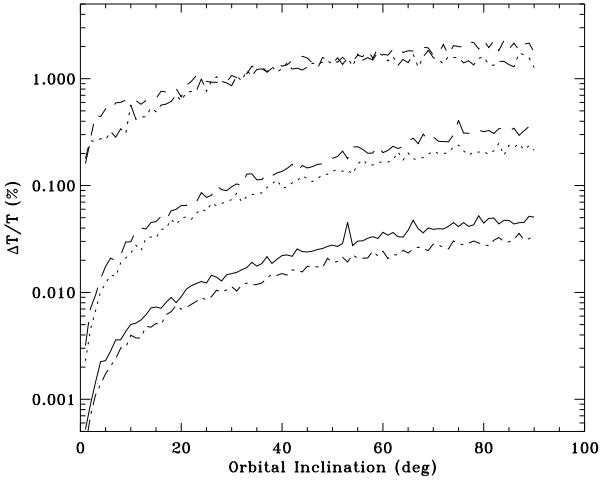
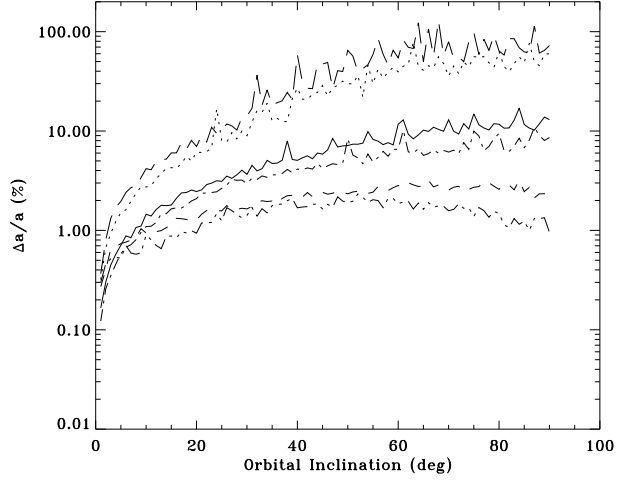
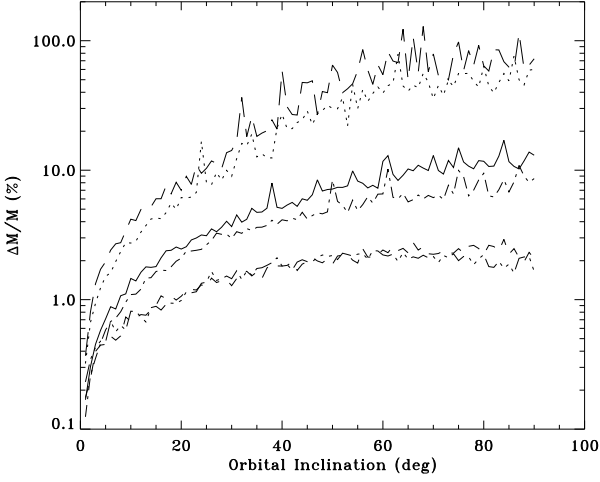




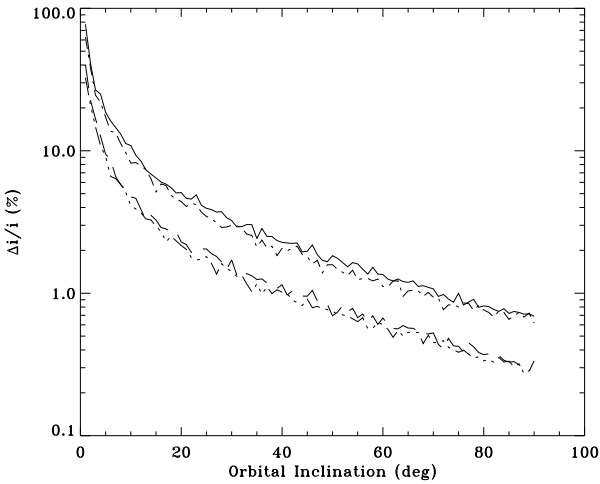
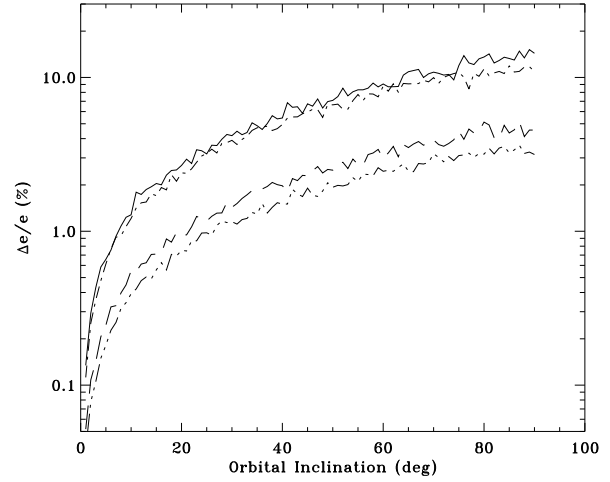
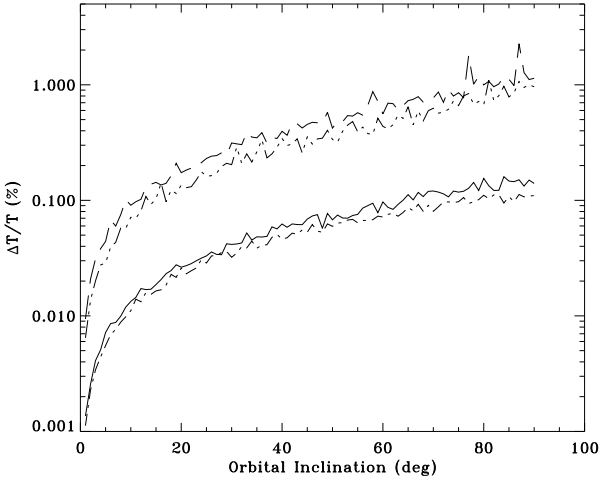
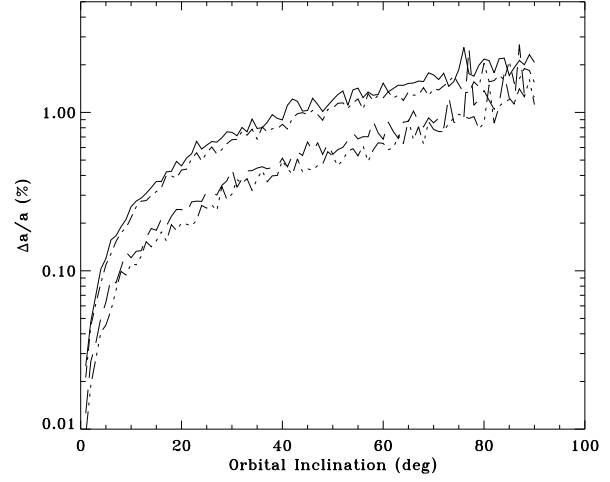
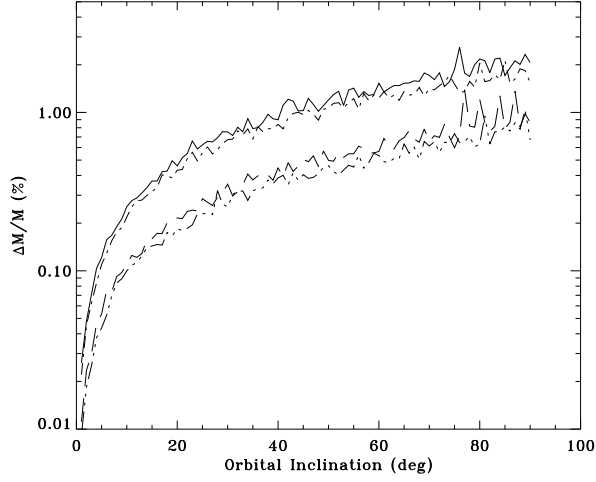








- $\text{---} : 55 \text{ Cnc b} \left\{ \begin{array}{l} T=0.04 \text{ yr} \\ M=0.84/\sin(i) M_{\text{J}} \\ \alpha=8/\sin(i) \mu\text{as} \end{array} \right.$
- $\text{- - -} : 55 \text{ Cnc c} \left\{ \begin{array}{l} T=0.12 \text{ yr} \\ M=0.21/\sin(i) M_{\text{J}} \\ \alpha=4/\sin(i) \mu\text{as} \end{array} \right.$
- $\text{---} : 55 \text{ Cnc d} \left\{ \begin{array}{l} T=14.7 \text{ yr} \\ M=4.05/\sin(i) M_{\text{J}} \\ \alpha=1917/\sin(i) \mu\text{as} \end{array} \right.$



--- : HD 12661 b $\left\{ \begin{array}{l} T=0.72 \text{ yr} \\ M=2.30/\sin(i) M_{\star} \\ \alpha=47/\sin(i) \mu\text{as} \end{array} \right.$
 --- : HD 12661 c $\left\{ \begin{array}{l} T=3.95 \text{ yr} \\ M=1.56/\sin(i) M_{\star} \\ \alpha=100/\sin(i) \mu\text{as} \end{array} \right.$

